SOME ASPECTS OF SURFACE WAVES ON ANTENNA STRUCTURES

by 1264

KUEN TIEN HWANG

B.S. Tatung Institute of Technology, Taipei, TAIWAN, 1966

A MASTER'S REPORT

submitted in partial fulfillment of the

requirements for the degree

MASTER OF SCIENCE

Department of Electrical Engineering

KANSAS STATE UNIVERSITY

Manhattan, Kansas

1970

Approved by

gary johnson

Major Professor

TABLE OF CONTENTS

CHAPTER 1

INTRODUCTION

1.1 Definition of Surface Wave. In order to define the term "surface wave", it is important to pay attention to the considerations that have led in the past to the definitions now generally accepted for other forms of guided electromagnetic waves. All these definitions are based on behavior in idealistic conditions. An example is the so-called T.E.M. wave propagating along a twin conductor transmission line where it is assumed that the guide is lossless.

The main characteristic feature of a surface wave is its nonradiating property and this should form the basis of its definition. In addition to this feature, it is usually assumed that the supporting surface representing the boundary between homogeneous media is straight in the direction of propagation of the wave, so that when curved surfaces arise they are regarded as perturbations. The definition suggested by Barlow and Brown (1962) for surface waves is the following: "A surface wave is one that propagates along an interface between two different media without radiation; such radiation being construed to mean energy converted from the surface-wave field to some other form". Another definition proposed by Zucker (Silver, 1963) for surface waves is as follows: A surface wave is a source-free solution of Maxwell's equations over an interface. It satisfies the radiation condition at infinity and boundary conditions at the interface. The basic principles of their definitions are based on physical and mathematical interpretations.

1.2. Previous Work in the Area. It has been known for more than 70 years, from a paper by Sommerfeld in 1899, that a ground-wave could propagate over a flat earth excited from a vertical dipole. This part of the total field he called 'surface wave'. Later his student Zenneck gave the appropriate solution of Maxwell's equations for the inhomogeneous plane wave over a flat surface with finite losses, which is the simplest form of surface wave. The interest taken in the subject was largely restricted to mathematical arguments until Goubau (1951) demonstrated the capabilities of the single-wire transmission line as a surface waveguide. Since 1952, many theoretical and practical investigations have been presented by many workers concerned with surface waves on antenna and surface waveguide structures. The common antenna structures are dielectric rods, corrugated rods, slotted waveguides, helices, Yagi-Uda arrays, dielectric sheets, corrugated surface ferrite and plasma sheets, and dipoles. Those surface waveguide structures are dielectric rods, dielectric cylinders, corrugated plane surfaces, corrugated conductors, dielectric-coated planes and dielectric coated wires. The details of waveguide structures and antenna structures have been collected and explained by Collin (1960) and Walter (1965) respectively. In 1965, Bobrovnikov, Goshin and Smirnov (1965) discussed the problem of excitation of radial cylindrical surface waves over metallic surfaces covered by a layer of dielectric or over corrugated surfaces. They observed that the low efficiencies of surface wave excitation can be improved by using concentric circular slots located on a dielectric conducting plane. Barlow (1967) has made a ferrite-loaded horn type of antenna which is capable of launching a 1.5 MHz surface wave over the earth.

1.3. Outline of this Report. The purpose of this report is to study the characteristics of surface waves on thin dielectric coated conducting planes and their effects on phased array antenna structures. At the same time, many practical problems concerned with excitation techniques are discussed.

Chapter II analyzes the characteristics of TM surface waves and TE surface waves on thin dielectric coated conducting planes by using Maxwell's equations. The wave impedances in different regions are also discussed.

In Chapter III, the effect of surface waves on similar phased array antenna structures is analyzed and discussed, based on various mathematical methods and experimental results. The physical phenomena of surface waves on phased antenna structures is also discussed.

In Chapter IV, several typical surface waves and their essential representive solutions of Maxwell's equations are shown. Also, several typical wave launchers are presented. Launching techniques and applications are explained briefly because many practical problems of launching and receiving need to be studied.

Chapter V gives a summary, and recommendations for further study. The conclusions of the results in Chapter II, Chapter III, and Chapter IV are presented. An experimental method to measure the efficiency of excitation of radical cylindrical surface waves is suggested.

CHAPTER II

CONDUCTING PLANE WITH A THIN DIELECTRIC COATING

2.1 TM Surface Wave And TE Surface Wave. Figure 2.1 illustrates a plane conducting surface, coated with a dielectric layer of thickness t, having a relative complex dielectric constant $\varepsilon_r = \varepsilon_r' - j\varepsilon_r''$. Let a TM wave be incident on the interface from the air region with H parallel to the interface. The incident wave has field components H_y, E_x, and E_z when the plane of incidence is in the x-z plane. Then the components of the electric field are given by

$$j\omega\varepsilon E_x = -\frac{\partial H_y}{\partial z} \tag{2.1a}$$

$$j\omega\varepsilon E_z = \frac{\partial H_y}{\partial x} \tag{2.1b}$$

In the free space region, the magnetic field has the form

$$H_y = A \exp(jh_1 x - j\beta z), \qquad x \geq t \tag{2.2}$$

where

$$h_1^2 + \beta^2 = K_0^2 = \omega^2 \mu_0 \varepsilon_0 \tag{2.2a}$$

In the dielectric region, the field consists of two waves propagating in the positive and negative x directions, and has the form

$$H_y = [B \exp(jh_2 x) + C \exp(-jh_2 x)]\, e^{-j\beta z}, \qquad 0 \leq x \leq t \tag{2.3}$$

where

$$h_2^2 + \beta^2 = \varepsilon_r K_0^2 = K^2 \tag{2.3a}$$

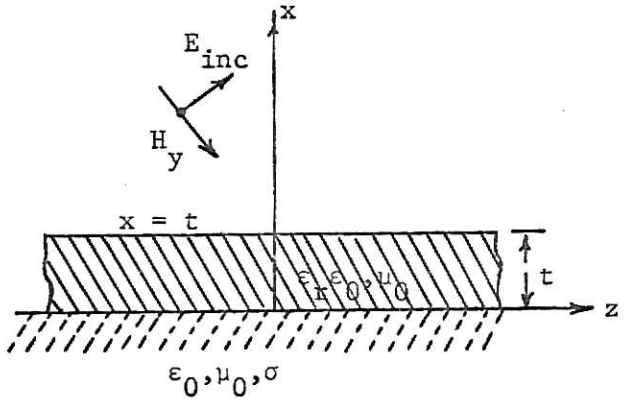

Figure 2.1 A conducting plane coated with a thin layer of dielectric.

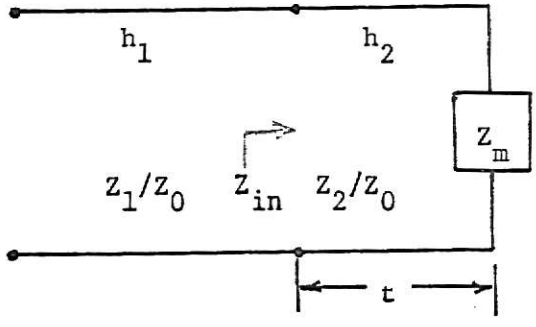

Figure 2.2 Equivalent transmission-line circuit for coated conducting plane.

The wave numbers h_1 and h_2 and the propagation constant β may be found by using the boundary condition at the free-space-dielectric interface and the dielectric-conducting plane interface (Collin, 1960). The wave impedances in the free space and dielectric regions are, respectively

$$Z_1 = \frac{Z_0 h_1}{K_0}, \qquad x \geq t \tag{2.4}$$

$$Z_2 = \frac{Z_0 h_2}{\epsilon_r K_0}, \qquad 0 \leq x \leq t \tag{2.5}$$

where

$$Z_0 = \sqrt{\mu_0/\epsilon_0}$$

and the normalized surface impedance looking from the dielectric to the metal is

$$Z_m = (1+j)\left(\frac{K_0}{2\sigma Z_0}\right)^{\frac{1}{2}}, \qquad t < 0 \tag{2.6}$$

where $\sigma >> \omega\epsilon$ is assumed. Combining these three wave impedances and transmission line theory, the equivalent transmission line circuit as shown in Figure 2.2 can be obtained.

If the normal input impedance at the air-dielectric interface is equal to Z_1/Z_0, there will be no reflection at the interface, and the incoming plane wave will become a surface wave. Conventional transmission- line theory (Collin, 1960) thus gives

$$\frac{Z_1}{Z_0} = Z_{in} = \frac{Z_2}{Z_0}\,\frac{Z_m + j(Z_2/Z_0)\tan h_2 t}{Z_2/Z_0 + jZ_m \tan h_2 t} \tag{2.7}$$

In this equation, one can make the approximation $Z_m = 0$, because it is very small at radio frequencies. It is also assumed that the thickness t is chosen so that $h_2 t$ is small. Now, by using equations (2.4), (2.5), and (2.7) one can obtain the normalized input impedance Z_{in} as

$$\frac{Z_1}{Z_0} = Z_{in} \simeq j\left(\frac{Z_2}{Z_0}\right) \tan h_2 t$$

$$\simeq j\left(\frac{Z_2}{Z_0}\right) h_2 t$$

$$\simeq j\left(\frac{Z_0 h_2}{\varepsilon_r K_0}\right) \frac{h_2 t}{Z_0} = j \frac{h_2^2 t}{\varepsilon_r K_0}$$

$$\simeq j \frac{(\varepsilon_r - 1) K_0}{\varepsilon_r} t \qquad (2.8)$$

Solving equations (2.1) and (2.8) one obtains

$$h_1 = \frac{Z_1}{Z_0} K_0 \simeq j\left(\frac{\varepsilon_r - 1}{\varepsilon_r}\right) K_0^2 t \qquad (2.9)$$

Thus a conductor coated with a thin layer of dielectric may be considered as a surface with a normalized surface impedance Z_s given by

$$Z_s = Z_{in} \simeq j \frac{(\varepsilon_r - 1)}{\varepsilon_r} K_0 t$$

$$= jX_s \qquad (2.10)$$

The propagation constant β is given by

$$\beta = (K_0^2 - h_1^2)^{1/2}$$

$$= \left[K_0^2 + \left(\frac{\varepsilon_r - 1}{\varepsilon_r} K_0^2 t\right)^2\right]^{1/2}$$

$$= K_0\left[1 + \left(\frac{\varepsilon_r - 1}{\varepsilon_r} t\right)^2\right]^{1/2} \tag{2.11}$$

The preceding analysis is valid only for a low-loss thin dielectric sheet over a highly conducting plane.

The TE surface wave is similar in structure to the TM surface wave, but the role of electric field and magnetic field is interchanged. For this case, Maxwell's equations reduce to

$$j\omega\mu_0 H_z = -\frac{\partial E_y}{\partial x} \tag{2.12}$$

$$j\omega\mu_0 H_x = \frac{\partial E_y}{\partial z} \tag{2.13}$$

Similarly one can also write

$$E_y = A \exp(jh_1 x - j\beta z), \qquad x \geq t \tag{2.14a}$$

$$E_y = [B \exp(jh_2 x) + C \exp(-jh_2 x)]e^{-j\beta z}, \qquad 0 \leq x \leq t \tag{2.14b}$$

where

$$h_1^2 + \beta^2 = K_0^2$$

$$h_2^2 + \beta^2 = \varepsilon_r K_0^2$$

The wave admittance is equal to

$$Y_1 = -\frac{H_z}{E_y} = \frac{Y_0 h_1}{K_0}, \qquad x \geq t \tag{2.15a}$$

$$Y_2 = \frac{Y_0 h_2}{\varepsilon_r K_0}, \qquad 0 \leq x \leq t \tag{2.15b}$$

$$Y_m = \left(\frac{K_0}{2\sigma Y_0}\right)^{\frac{1}{2}} (1+j), \qquad x \leq 0 \tag{2.15c}$$

where $Y_0 = \frac{1}{Z_0}$

Similarly to the TM case, if the normal input admittance at the air-dielectric interface is equal to Y_1/Y_0, then there will be no reflection at the interface and the incoming TE plane wave will become a surface wave. Conventional transmission line theory gives

$$\frac{Y_1}{Y_0} = Y_{in} = \frac{Y_2}{Y_0} \frac{Y_m + j(Y_2/Y_0) \tan h_2 t}{Y_2/Y_0 + j\, Y_m \tan h_2 t} \tag{2.16}$$

By the same assumptions and approximations used for the TM surface wave, one can obtain the input surface admittance and the wave number h_1 as

$$Y_{in} \simeq j \frac{\varepsilon_r - 1}{\varepsilon_r} K_0 t = jB_{in} \tag{2.17}$$

$$h_1 \simeq j \frac{\varepsilon_r - 1}{\varepsilon_r} K_0^2 t \tag{2.18}$$

Therefore, from equations (2.17) and (2.18) it is seen that a conductor coated with a thin layer of dielectric may be regarded as

a surface with a normalized surface admittance Y_s given by

$$Y_s = Y_{in} \cong j \frac{\varepsilon_r - 1}{\varepsilon_r} K_0 t \tag{2.19}$$

$$= jB_s$$

2.2 Discussion of TM and TE Surface Wave Characteristics On a Coated Conducting Plane. From the analysis of the last section as indicated in equations (2.10) and (2.19) one can see that TM surface waves exist over a surface with a surface impedance having an inductive term, while TE surface waves exist over a surface with a surface impedance having a capacitive term. According to equations (2.2) and (2.9) one can find that the TM field has exponential decay normal to the surface if the reactive part of impedance is inductive. The larger the inductance of the surface, the more closely will the wave be bound to the surface. Also, if the dielectric layer is thick, the field will be tightly bound to the surface. Conversely, the field will be loosely bound to a thin dielectric layer. From equation (2.11), one can find that the phase velocity is less than the velocity in free space for a surface wave supported by a highly inductive surface.

CHAPTER III

SURFACE WAVES ON PHASED ARRAY ANTENNAS

3.1 Introduction. In recent years, many workers have found that the element patterns of certain types of phased arrays exhibited nulls and dips at specific scan angles. These nulls and dips are related to the presence of guided waves supported by the array surface (Knittel, Hessel, and Oliner, 1968). The element pattern of an array of coaxial horns covered by individual dielectric radomes was obtained by Lechtreck, (1968). A pattern, measured at the Bendix Corporation, of an array of open-ended waveguides arranged in a triangular lattice in a conducting plane has been published by Farrell and Kuhn (1966). Each of these element patterns has a dip at an angle closer to broadside than that predicted by array theory alone. The shallowness of the dips obtained in these measurements is due to the fact that the arrays are small; if the arrays are infinite in extent, the dips will become nulls.

There are also other kinds of evidence for the existence of this unusual null in element patterns from theoretical calculations and from wave-guide simulator experiments. Farrell and Kuhn (1966) have performed theoretical calculations which verified the experimental behavior of "brick" arrays. Diamond (1967) has computed an element pattern for an array of open-ended square waveguides in a conducting plane which shows the null.

Those efforts have gradually been expanded by many workers. Galindo and Wu (1968) have studied the effect of the dielectric geometry, dielectric constant, and sheath thickness on the wide angle performance of an array of rectangular waveguides. Later, Wu and Galindo (1968) used a dielectric sheathed phased array of rectangular waveguides to analyze the influence of dielectric thickness, dielectric constant and waveguide wall thickness on the null location and the relationship between the null phenomenon and surface waves. They also presented some further results for thin sheaths and multiple sheaths. Nagelberg (1968) has shown, both theoretically and experimentally, the radiating characteristic of an aperture- type antenna covered by a dielectric sheath. He also predicted that the principal effect of the thickness of the dielectric is a significant broadening of the radiation pattern over a narrow frequency band, in which a surface wave is excited and propagates along the dielectric slab.

Knittel, Hessel, and Oliner (1968) have investigated the basic causes of these element pattern nulls, and have clarified the relationship between these nulls and possible guided waves. Surface waves and leaky waves which may be supported by the phased array face itself have also been found.

In this chapter the primary concern will be with some literature published in recent years. Various methods have been used in discussing similar structure problems theoretically and experimentally. The array structure, which is analyzed in detail by using the unit cell and equivalent network technique method, Fourier transform method, and integral equation method will be studied in sections 3.2, 3.3 and 3.4, respectively.

3.2 Unit Cell and Equivalent Network Method. Figure 3.1 consists of an array of slots or apertures in a conducting plane, fed from below with rectangular waveguides and covered above by a dielectric slab. In order to study the basic characteristics of external resonances, the angle dependent resonance of the structure external to the waveguides, the array structure is chosen as a two dimensional array of narrow slots fed by parallel plate waveguides, Figure 3.2. This can not only simplify the prototype of the structure and retain the basic features, but also can avoid complications in description. Therefore, the structure will be considered infinite in the x and y directions. It is assumed that a TEM mode is incident from below in the parallel plate waveguides. These modes are matched to the respective waveguides. The generators are identical. The amplitude of the incident mode in each waveguide is the same, but the phases will generally be different. A plane wave then is radiated into the space above the array at an angle θ. The scan angle is in the x-z plane and the E-field of the radiated wave is also in the x-z plane. The array is infinite, so one can use the unit cell technique to solve the infinite periodic structure (discussed in detail by Oliner and Malech (1966)). It is two dimensional, so that one can confine scanning to one plane and thus simplify the analysis. It is the simplest kind of array utilizing aperture radiating elements, so that one can clearly distinguish the external and the internal portions of the array. If the slot width is kept very small, say $d/B < 0.1$, an equivalent network is easily derived and can be used to show the existence of the resonance and its important characteristics. The E-plane scan is the most useful scan

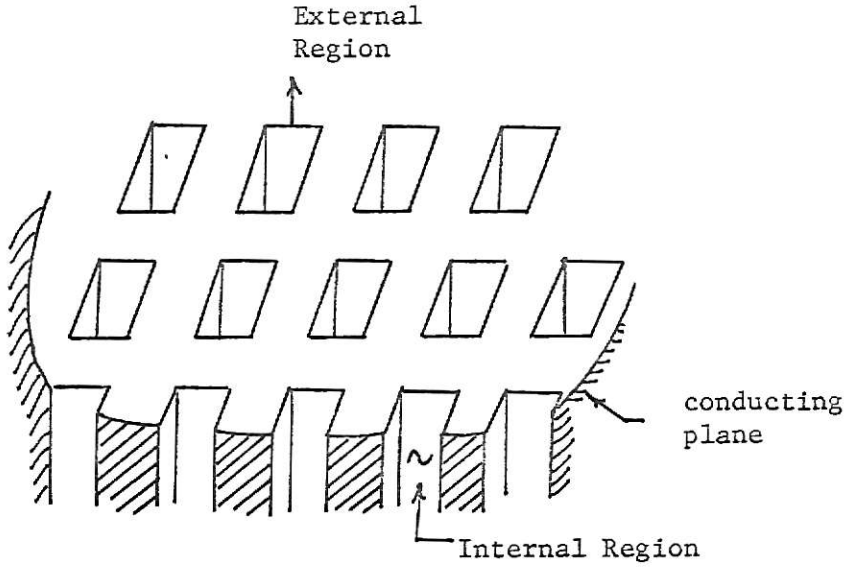

Figure 3.1 Array of aperture elements in conducting plane

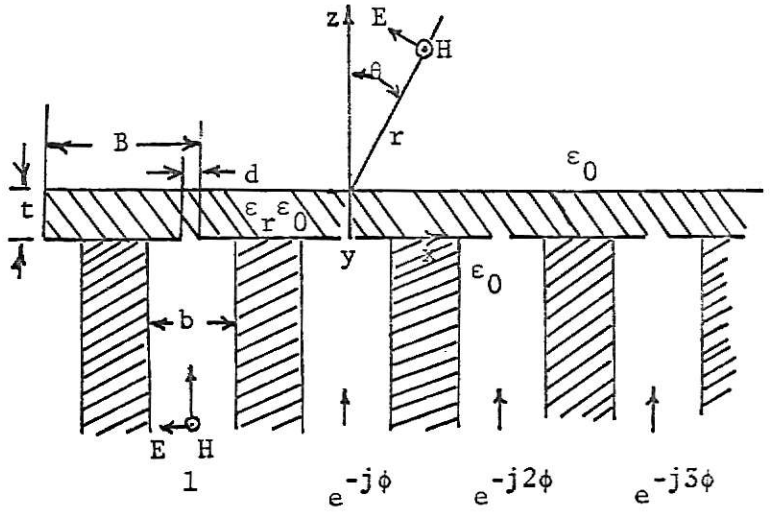

Figure 3.2. Array of narrow slots fed by parallel-plate waveguides and covered by dielectric slab.

plane to be chosen for a study of external resonance, since one finds an E-plane scan resonance only for a thin dielectric slab. In the H-plane scan, however, a thick dielectric slab is required for a resonance (Oliner and Malech, 1966).

To derive an equivalent network for the structure in Figure 3.2, one first forms the unit cell of the aperture as shown in Figure 3.3. Then one can find an equivalent network for the junction of two waveguides with one of them covered with a dielectric layer of finite thickness, if one knows the form of the electric field in the aperture at all scan angles.

If it is assumed that the slots in the array in Figure 3.2 are chosen to be sufficiently narrow, and there are N propagation modes, then, their radiation power can be written as

$$P = \sum_{n=0}^{N} Y_{un} \mid V_{un} \mid^2 \tag{3.1}$$

where V_{un} = modal voltage in the unit cell

Y_{un} = modal admittance in the unit cell

We may also define the symbols

$\bar{e}_{un}$ = unit cell vector mode function

$\bar{e}_f$ = feed wave guide vector mode function

V_f = excited voltage furnished by waveguide

Y = input characteristic admittance of unit cell seen by the TEM mode traveling in the positive z direction in the feed guide.

$\bar{E}_t$ = transverse electric field in the slot

The input characteristic admittance Y can be defined as

$$Y = \frac{\text{radiated power}}{|V_f|^2} + \frac{\text{stored power}}{|V_f|^2} \tag{3.2}$$

The voltage terms in equations (3.1) and (3.2) can be defined in terms of the vector mode functions (Oliner and Malech, 1966), for example,

$$V_f = \iint_{\text{slot}} \bar{E}_t \cdot \bar{e}_f^* \, dS \tag{3.3}$$

where $\bar{e}_f^*$ is the complex conjugate of $\bar{e}_f$.

For the E-plane scan, the unit cell vector mode function $\bar{e}_{un}$ and feed wave guide vector mode function $\bar{e}_f$ are given by Oliner and Malech, (1966) as

$$\bar{e}_{un} = \frac{\bar{a}_x}{\sqrt{B}} \exp(jK_{xn}x) \tag{3.4}$$

$$\bar{e}_f = \frac{\bar{a}_x}{\sqrt{b}}$$

where

$$K_{xn} = K_0 \sin\theta + \frac{2\pi n\lambda}{B}, \qquad n = 0, +1, +2, +3, \ldots + N \tag{3.4a}$$

Since the tangential field exists only over the aperture and is zero at the other points in the aperture plane, the integration is performed only over the slot. From equations (3.3) and (3.4) one finds that

$$|V_{un}| = \left| \iint_{slot} \bar{E}_t \cdot \bar{e}^*_{un} \, dS \right|$$

$$= \left| \frac{2E_0}{\sqrt{B}} \frac{\sin(K_{xn} d/2)}{K_{xn}} \right| . \tag{3.5}$$

$$|V_f| = \left| \iint \bar{E}_t \cdot \bar{e}^*_f \, dS \right| = \frac{|E_0|}{\sqrt{b}} d \tag{3.6}$$

where $\bar{E}_t = E_0 \, \bar{a}_x$ (3.7)

d = width of slot

Hence

$$\left| \frac{V_{un}}{V_f} \right|^2 = \left| \frac{b}{B} \left(\frac{\mathrm{Sin}(K_{xn} d/2)}{K_{xn} d/2} \right)^2 \right| \tag{3.8}$$

By substituting equation (3.8) into (3.2), one can obtain

$$Y = \sum_{n=0}^{N} \frac{b}{B} \left(\frac{\sin(K_{xn} d/2)}{K_{xn} d/2} \right)^2 Y_{un} + jB_{in} \tag{3.9}$$

Equation (3.9) can be simplified by defining the term Y_{in} as

$$Y_{in} = \left(\sqrt{\frac{b}{B}} \frac{\sin(K_{xn} d/2)}{K_{xn} d/2} \right)^2 Y_{un}$$

$$= (T_n)^2 \, Y_{un} \tag{3.10}$$

where

$$T_n = \sqrt{\frac{b}{B}} \frac{\sin(K_{xn} d/2)}{K_{xn} d/2} \qquad n = 0, 1, 2, \ldots, N$$

Thus, the TEM mode input admittance Y can be expressed in the form

$$Y = \sum_{n=0}^{N} (T_n)^2 Y_{un} + jB_{in} \qquad (3.11)$$

$$= \sum_{n=0}^{N} Y_{in} + jB_{in}$$

B_{in} is the susceptance resulting from the stored power in the cut off modes on the inside of the aperture and can be approximately expressed as (Knittel, Hessel and Oliner 1968).

$$B_{in} = j \frac{2b}{\lambda} Y_0 \, \&n \csc \left(\frac{\pi d}{2b}\right)$$

The dielectric in the unit cell waveguide is of thickness t, and air fills the unit cell for z > t. The electric field in the unit cell is parallel to the plane of incidence (E-plane scan), so that the wave admittances for the nth mode in the dielectric region and free space are, respectively

$$Y_{n\varepsilon} = \frac{\omega \varepsilon_r \varepsilon_0}{K_{n\varepsilon}} \qquad 0 \leq z \leq t \qquad (3.11a)$$

$$Y_n = \frac{\omega \varepsilon_0}{K_n} \qquad z \geq t \qquad (3.11b)$$

where

$$K_{n\varepsilon} = \sqrt{\varepsilon_r K_0^2 - K_{xn}^2} \qquad (3.11c)$$

$$K_n = \sqrt{K_0^2 - K_{xn}^2} \qquad (3.11d)$$

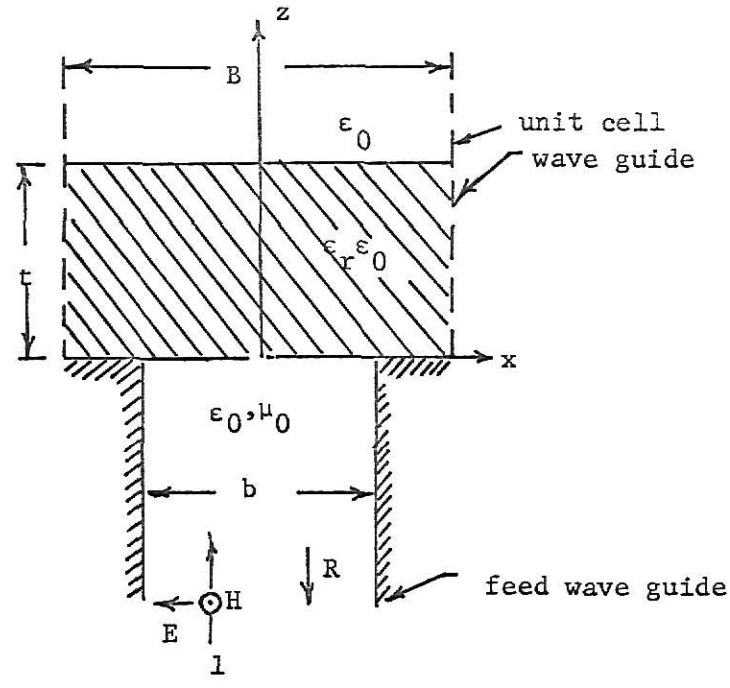

Fig. 3.3 Unit cell for the array of Figure 3.2.

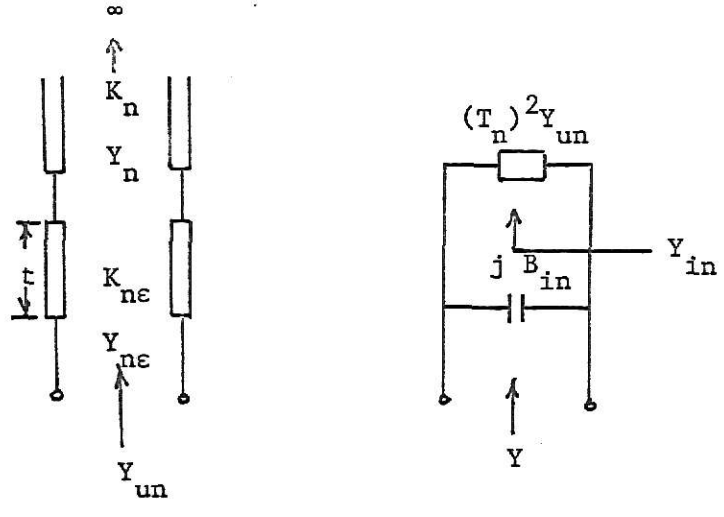

(a) Equivalent circuit for nth modes for unit cell

(b) Equivalent Network for TEM mode without ideal transformer.

Figure 3.4

where $K_{n\varepsilon}$, and K_n are the wave numbers of the n-th mode in the z-direction in the dielectric and air respectively, ε_r is the relative permittivity of the dielectric, and $K_0 = \omega\sqrt{\mu_0\varepsilon_0}$ is the free-space wave number. The parameter K_{xn} is the wave-number of the n-th mode in the x-direction and is related to the scan angle. The mode index is n. Combining the two wave admittances, $Y_{n\varepsilon}$ and Y_n, and transmission line theory (Collin, 1960), one can obtain the equivalent transmission line circuit as in Figure 3.4(a). From the transmission line circuit representation, one can determine the nth mode input admittance in the unit cell in the positive z direction as

$$Y_{un} = Y_{n\varepsilon} \frac{jY_{n\varepsilon} + Y_n \cot(K_{n\varepsilon}t)}{Y_{n\varepsilon}\cot(K_{n\varepsilon}t) + jY_n} \tag{3.12}$$

Then, substituting equation (3.12) into equation (3.9) one obtains the TEM mode input admittance of the unit cell as

$$Y = \sum_{n=0}^{N} \frac{b}{B} \left(\frac{\sin(K_{xn}d/2)}{K_{xn}d/2} \right)^2 Y_{n\varepsilon} \frac{jY_{n\varepsilon} + Y_n\cot(K_{n\varepsilon}t)}{Y_{n\varepsilon}\cot(K_{n\varepsilon}t) + jY_n} + jB_{in} \tag{3.13}$$

It is well known that the array input admittance Y is related to the array reflection coefficient R by

$$R = \frac{Y_0 - Y}{Y_0 + Y} \tag{3.14}$$

where Y_0 is the characteristic admittance of the TEM mode in the feed waveguide and $Y_0 = \sqrt{\frac{\varepsilon_0}{\mu_0}}$.

Equation (3.11) can be expressed in the form of the equivalent network as shown in Figure 3.4(b) in which there is no transformer and

the Y_{in} term is chosen as T_n^2 times the unit cell input admittance Y_{un}. For the purpose of changing the equivalent network admittance level, one can use an ideal transformer $(1:T_n)$ to cascade with the unit cell input admittance Y_{un} and consider Y_{in} as the ideal transformer input admittance as shown in Figure 3.4(c). Y_{in} still has the same characteristics. Then, one can parallel jB_{in} to Y_{in} and express equation (3.9) in the form of the equivalent network as shown in Figure 3.4(c). The n = 0, and n = 1 mode transmission lines are the essential ones in the external resonance phenomenon. All the other higher modes outside the aperture are assumed to be below cut-off in both dielectric and air and are lumped together as a susceptance B_{hn} (where the subscript signifies 'higher modes') which is given by

$$jB_{hn} = \sum_{n=2}^{N} (T_n)^2 \, Y_{n\varepsilon} \frac{jY_{n\varepsilon} + Y_n \cot(K_{n\varepsilon} t)}{Y_{n\varepsilon} \cot(K_{n\varepsilon} t) + j\, Y_n} \tag{3.15}$$

An equivalent circuit for equation (3.15) has been obtained by Oliner and Malech (1966), but they do not give an explicit relation between B_{hn} and T_n, since they were concerned only with the particular scan angle for $|R| = 1$ and not with the variation of $|R|$ about this angle. The purpose of choosing a small aperture is that the electric field in the x-direction is constant for all scan angles, so that B_{in} is independent of scan angle and T_n is only slightly dependent.

Because only two external modes are important in the array, one can estimate the qualitative features of the reflection coefficient versus scan angle from the equivalent network. For making the phased array in Figure 3.2 into a practical phased array, it is necessary to

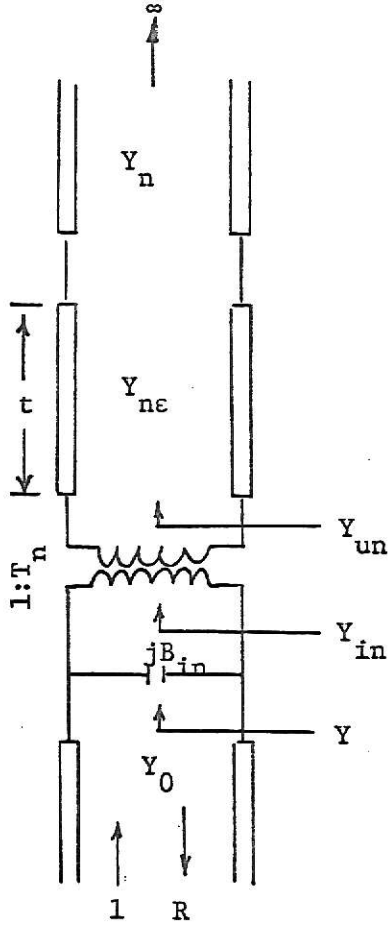

Figure 3.4 (c) Equivalent Network for a TEM mode in the unit cell of the array

include a matching network to match the admittance of the array to that of the feed guide at broadside scan. This can be done in practice by adding an appropriate iris (susceptance and transformer) to change the b-dimension of the feed guide a half wavelength below the aperture plane. In the equivalent network, this is the same as adding the susceptance and transformer at the aperture. The latter can be done as shown in Figure 3.5. In this figure, B_M is the sum of three susceptances,

$$B_M = B_{in} + B_{hn} + B_{ex} \tag{3.16}$$

where B_{ex} is the extra susceptance added for matching. B_{hn} is the total higher model susceptance when all the higher modes outside the aperture are assumed to be below cutoff in both dielectric and air. T_M in Figure 3.5 is the transformer added for matching, and $T_0 \simeq T_1 \simeq \sqrt{\frac{b}{B}}$ as d is very small.

One can find that B_M varies slightly with θ and that this variation is mostly due to the n = +2 mode. If this mode is removed from B_M and displayed explicitly, the variation in the resulting B_M with θ is almost zero. By using the simplified equivalent network as shown in Figure 3.6, one can more accurately obtain the performance of the phased array based on three external modes and one internal (TEM) mode. B_N is the susceptance which can cancel the susceptance from the external mode transmission lines at $\theta = 0$. T_N is just the transformer which transforms the conductance from the n = 0 transmission line at $\theta = 0$ to the characteristic admittance of the feed guide.

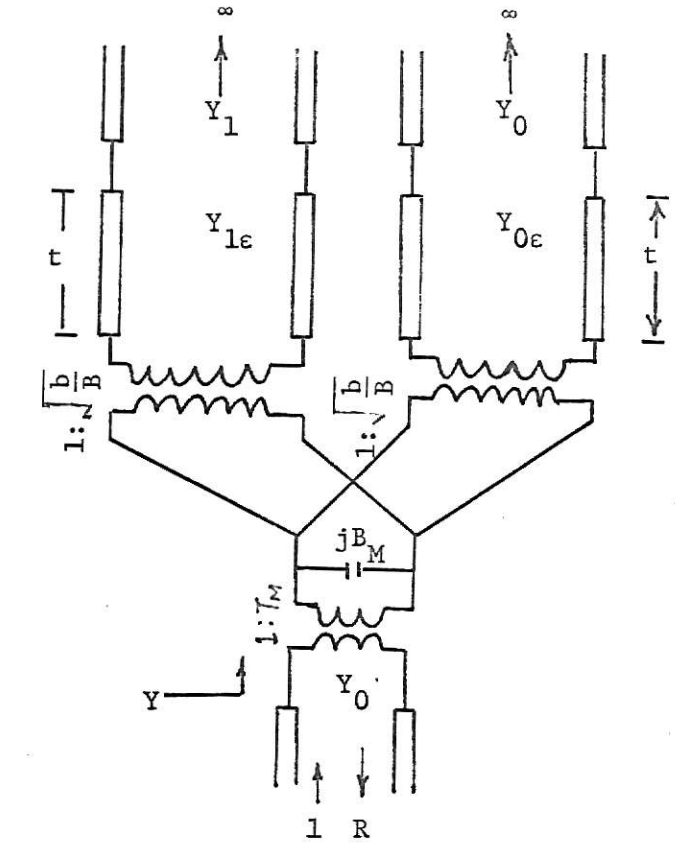

Figure 3.5 Equivalent network for array in Fig. 3.4 after matching at broadside. Only two modes are shown.

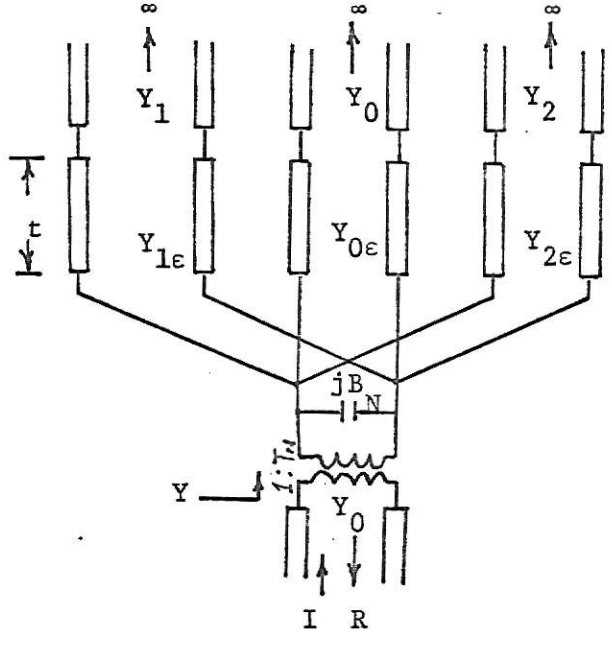

Figure 3.6 Simplified equivalent network utilizing only three external modes.

The equivalent network derived in the preceding analysis yields the array reflection coefficient R when all the elements of the array are excited. It also yields the transmission coefficient T for a beam radiating into space. It has been shown by Oliner and Malech (1966) that for a lossless array radiating a single beam, $|R(\theta)|$ is related to the element pattern via

$$g_e = [1 - |R(\theta)|^2] \cos \theta \tag{3.17}$$

where g_e is the realized gain of one element in the array with all other elements terminated in their generator admittances. If $R(\theta)$ is zero, g_e equals 1 for broadside match. If there is more than one radiating beam, or if the array aperture region contains lossy material, it is easy to show that equation (3.17) can be replaced by

$$g_e = |T(\theta)|^2 \cos \theta \tag{3.18}$$

where $T(\theta)$ is the ratio of power transmitted into the air in the unit cell to the power incident in the feed waveguide. If $T(\theta)$ is given, then one can compute g_e.

One can ascertain from the equivalent network in Figure 3.5 that there is a null in the element pattern and that the direction of this null changes with dielectric thickness. This may be argued as follows. If $t = 0$, then, from equation (3.11b), Y_1 is infinite at a scan angle for which $K_1 = 0$. This scan angle θ (shown in Figure 3.2) is equal to $\sin^{-1}(1 - \frac{\lambda}{B})$. Since the modal transmission lines are in shunt at the aperture, the total input admittance Y is infinite. It places a short circuit across the $n = 0$ line and causes complete reflection, therefore, a null occurs in the pattern. If $t > 0$ and the scan angle is still at the

same angle for which $K_1 = 0$, then, from the equations (3.11a), (3.11b) and (3.11c) one can find that Y_1 is infinite and $Y_{1\varepsilon}$ is finite. Therefore, $Y_1 = \infty$ places a short circuit at the $Y_{1\varepsilon}$ output terminal and the n = 1 line input admittance becomes finite. After transformer transformation, this finite admittance is parallel to the n = 0 line input admittance and the total input admittance Y becomes finite. When the scan angle θ (as shown in Figure 3.2) is larger than the scan angle θ for which $K_1 = 0$, from equations (3.11a), (3.11b), (3.11c), (3.11d) and (3.4a), one can find that Y_1 becomes a capacitive susceptance, and $Y_{1\varepsilon}$ is still a conductance. When this scan angle θ is increased to $\theta = \sin^{-1}\left(\frac{t}{\lambda}(\sqrt{\varepsilon_r - 1} - \frac{\lambda}{B}\right)$, one can find that the denominator of equation (3.12) for n = 1 will become zero. Therefore, the input admittance for the n = 1 line becomes infinite. After transformer transformation, this infinite admittance is parallel to the n = 0 line input admittance and the total input admittance Y is infinite. This infinite input admittance will cause complete reflection. Thus a null occurs in the pattern at this scan angle, $\theta = \sin^{-1}\left(\frac{t}{\lambda}\sqrt{\varepsilon_r - 1} - \frac{\lambda}{B}\right)$.

From equations (3.11a) and (3.11c), one can find that $Y_{1\varepsilon}$ is infinite at the scan angle for which $K_{1\varepsilon} = 0$. This scan angle θ is equal to $\sin^{-1}(\varepsilon_r - \frac{\lambda}{B})$. Thus, the n = 1 line input admittance is also infinite for this θ. After transformer transformation, this infinite input admittance is parallel to the n = 0 line input admittance and the total input admittance Y becomes infinite. This infinite input admittance Y will cause complete reflection. Thus, another null occurs in the pattern at this scan angle, $\theta = \sin^{-1}(\varepsilon_r - \frac{\lambda}{B})$.

The element pattern which exhibits multiple nulls for the array in Fig. 3.2 with $B/\lambda = 0.5$, $t/\lambda = 0.5$, $\varepsilon_r = 2.56$, $b/\lambda = 0.3$ (Knittel, Hessel and Oliner, 1968), is shown in Figure 3.7. Figure 3.8 shows the relationship between reflection coefficients and element patterns with different slab thicknesses for the array in Figure 3.2 with $B/\lambda = 0.5$, $\varepsilon_r = 2.56$ and $b/\lambda = 0.3$.

It is known that the reflection coefficient magnitude $|R|$ is equal to unity at a particular scan angle corresponding to the element pattern null. For this condition all power from the source is reflected back from the aperture, and the dominant mode input admittance Y becomes infinite at the aperture or $\frac{n\lambda}{2}$ away from the aperture plane. At the aperture plane, higher modes are present; however, at a plane $\lambda/2$ below the aperture plane it is safe to assume that only the dominant-mode exists, so that a short circuiting plate may be placed there without disturbing the field. The resulting structure is seen in Figure 3.9 to be a dielectric layer placed on a type of corrugated surface.

The approximate analysis presented herein of the array of Figure 3.2 has assumed that a constant field which is independent of scan angle can exist in the aperture. This field has been given as

$$\bar{E}_{ap} = E_0 \, \bar{a}_x \tag{3.19}$$

therefore, the magnitude of the dominant-mode voltage in the aperture plane becomes

$$|V_{f0}| = \frac{|E_0|}{\sqrt{b}} \, d \tag{3.20}$$

as in equation (3.6). Because the dominant-mode admittance is infinite, this dominant-mode voltage must be zero in the aperture plane and E_0 must

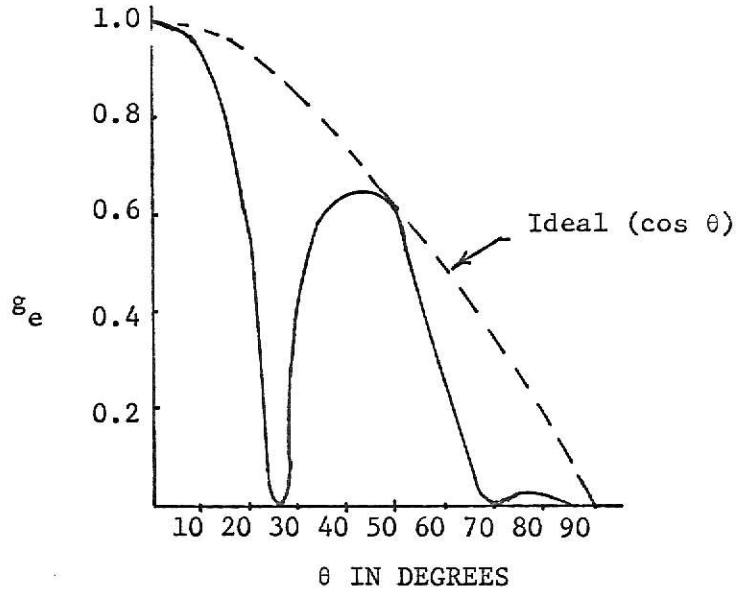

Figure 3.7. Element pattern exhibiting multiple nulls for the array in Figure 3.2 with a thick dielectric layer; $B/\lambda = 0.5$, $t/\lambda = 0.5$, $b/\lambda = 0.3$

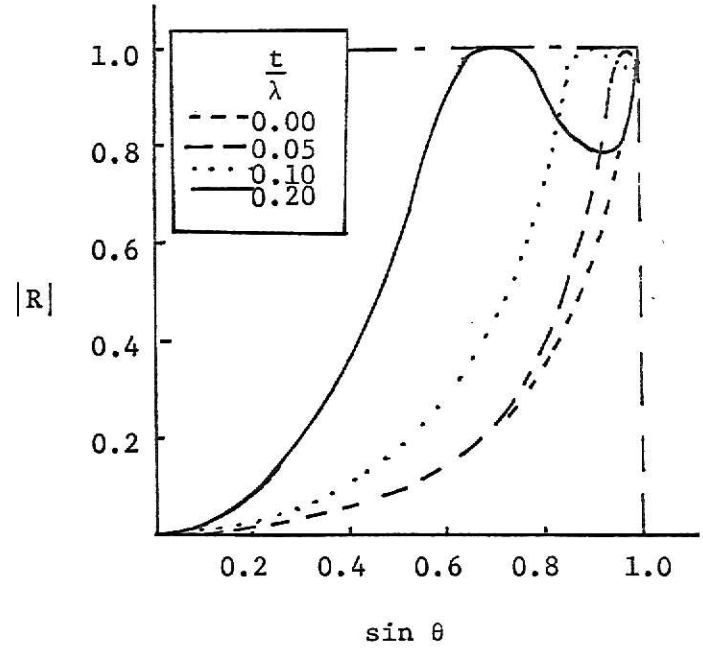

Figure 3.8 Reflection Coefficients and element patterns for various thickness t with $B/\lambda = 0.5$, $\varepsilon_r = 2.56$, $b/\lambda = 0.3$

be zero. Hence, according to this approximation, the total electric field in the aperture would vanish and a short circuit may be placed, as in Figure 3.10, actually closing off the slots.

If denominator of equation (3.12) equals to zero, then it is regarded as the condition on the first higher mode which corresponds to $|R| = 1$. It is also consistent with the transverse resonance condition for a TM surface wave on a dielectric slab placed on a perfectly conducting plane.

The above discussion has indicated that at the particular scan angle corresponding exactly to the element pattern null one may place short circuiting plates at an appropriate location in the feed guides, as shown in Figure 3.9, except that their distance from the aperture plane will differ from $\lambda/2$ for wider apertures. Under this condition, the total field existing on the array face is identical to a surface- wave mode of the dielectric-loaded corrugated structure as shown in Figure 3.9. Such a corrugated surface has long been known as a structure which is able to support surface waves. This structure is a periodic structure and can support only the TM surface wave in the absence of a dielectric material. The period of corrugation should be less than a half free space wave length in order to support the TM surface wave. But if there is a dielectric slab cover on the array aperture or corrugated surface, it can not only support a TM surface wave but also a TE surface wave. Therefore a surface wave can exist on this array structure.

3.3 Fourier Transform Method. This method determines the far-zone radiation properties of an aperture covered by a dielectric sheath

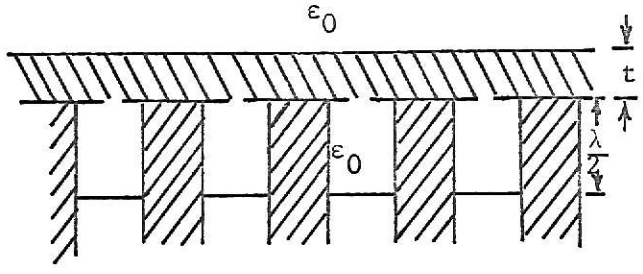

Fig. 3.9. Dielectric-loaded corrugated structure formed by plates $\lambda/2$ below the aperture plane

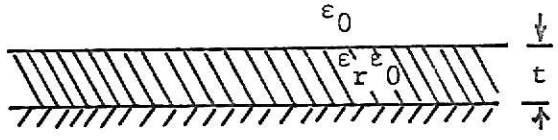

Figure 3.10 Dielectric slab on a perfect conducting plane formed by closing off the aperture

as shown in Figure 3.11. It is assumed that the electric field is in the y-direction and that all the quantities are independent of y. In addition to its mathematical simplicity, this two dimensional situation can be realized experimentally by erecting parallel conducting planes perpendicular to the electric field (Nagelberg, 1968).

Using a plane wave (Fourier) spectrum to represent the field, E_y can be expressed by

$$E_y(x,z) = \frac{1}{2\pi} \int_{h=-\infty}^{+\infty} G(x,h) e^{jhz}\, dh \tag{3.21}$$

$$G(x,h) = \int_{z=-\infty}^{+\infty} E_y(x,z) e^{-jhz}\, dz \tag{3.22}$$

where h, the transform variable, denotes the z-direction propagation constant of the particular plane wave component.

The function G(x,h) satisfies the two-dimensional wave equation,

$$\frac{d^2G(x,h)}{dx^2} + \beta^2 G(x,h) = 0 \tag{3.23}$$

where $\beta = (K^2 - h^2)^{1/2}$ inside the sheath, $\beta = \beta_0 = (K_0^2 - h^2)^{1/2}$ outside the sheath, with K and K_0 being the respective wave numbers. If the proper Riemann surface is chosen as shown in Figure 3.12, the square root can be defined as

$$\beta = + (K^2 - h^2)^{1/2} \qquad h \text{ real}, \quad K > |h| \tag{3.24a}$$

$$\beta = + j(h^2 - K^2)^{1/2} \qquad h \text{ real}, \quad K < |h| \tag{3.24b}$$

The conditions given by equations (3.24a) and (3.24b) are based on the following physical requirements: (i) waves radiated far from the aperture

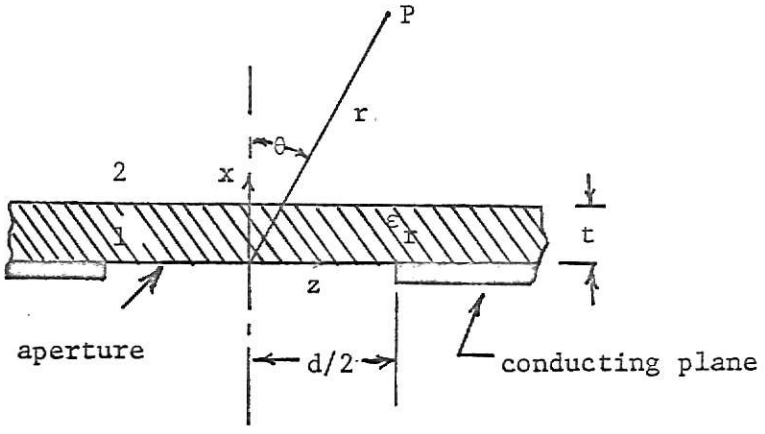

Figure 3.11 Aperture of width d bounded by ground plane and covered by a dielectric sheath of thickness t and dielectric constant ε_r.

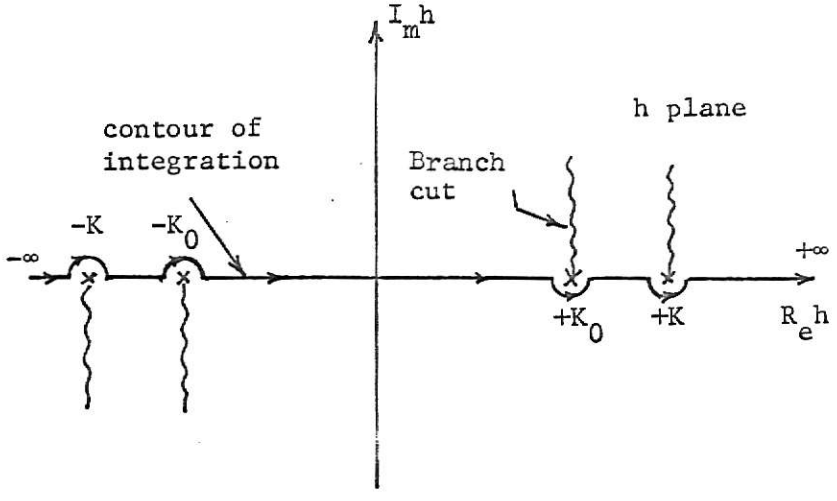

Figure 3.12 Definition of proper Riemann surface for evaluation of $\beta_0 = (K_0^2 - h^2)^{1/2}$ and $\beta = (K^2 - h^2)^{1/2}$.

travel in the +x direction and (ii) slow waves propagating in the $\pm z$ direction decrease exponentially in amplitude with respect to distance from the dielectric sheath. The boundary conditions for solving this problem can be regarded as

$$G(0,h) = G_0(h) \tag{3.25a}$$

$$G, \text{ and } \frac{\partial G}{\partial x} \text{ are continuous at } x = t \tag{3.25b}$$

where $G_0(h)$ is the Fourier transform of the aperture illumination.

The principal interest is in region 2, outside the sheath, where the transform function can be denoted by

$$G_2(x,h) = A(h)e^{j\beta_0 x} \tag{3.26a}$$

In a similar manner the field in region 1, inside the dielectric sheet, can be represented as

$$G_1(x,h) = B(h)e^{j\beta x} + C(h)e^{-j\beta x} \tag{3.26b}$$

Solving equations (3.26a) and (3.26b) with the boundary conditions given by equations (3.25a) and (3.25b) yields

$$A(h) = \frac{G_0(h)\ \exp(-j\beta_0 t)}{\cos \beta t - j \frac{\beta_0}{\beta} \sin \beta t} \tag{3.27}$$

And by substituting equations (3.26) and (3.27) into equation (3.21), one obtains

$$E_y(x,z) = \frac{1}{2\pi} \int_{h=-\infty}^{+\infty} \frac{G_0(h)\ \exp(-j\beta_0 t)}{\cos \beta t - j \frac{\beta_0}{\beta} \sin \beta t} \exp\ (j\beta_0 x)\ \exp\ (jhz)\ dh \tag{3.28}$$

The determination of the far-zone radiation pattern is made by using the integral form given by equation (3.28) and proceeds by saddle point integration. First, one transforms equation (3.28) into the polar coordinates r, and θ as shown in Figure (3.11). The coordinates r and θ are related to x, z by

$$\begin{aligned} x &= r \cos \theta \\ z &= r \sin \theta \end{aligned} \tag{3.29}$$

Next, using the transformation $h = K_0 \sin \alpha$, equation (3.28) can be written

$$E_y (r,\theta) = \frac{1}{2\pi} \int_c F(\alpha) \exp [jK_0 r \cos (\alpha-\theta)] \cos\alpha \, d\alpha \tag{3.30}$$

where the new contour is given in Figure 3.13. In the transformation from the h-plane to the α-plane, the integral becomes independent of the sign of the square root, therefore the branch cuts disappear.

To compute the field, one can let $K_0 r \to \infty$ and use the saddle point method to determine an asymptotic formula for the integral.

For the purpose of finding the radiation pattern only, it is sufficient to observe that the saddle point occurs at $\alpha = \theta$. Therefore, the angular variation of field can be specified in terms of a function of θ as

$$G(\theta) = G_0(K_0 \sin \theta) \cos \theta \cdot T(\theta) \tag{3.31}$$

where T(θ), the sheath transmission pattern, (Nagelberg, 1968) is given by

$$T(\theta) = \frac{\exp (-jK_0 t \cos \theta)}{\cos [K_0 t(\varepsilon_r - \sin^2\theta)^{1/2}] - \dfrac{j \cos \theta}{(\varepsilon_r - \sin^2\theta)^{1/2}} \sin [K_0 t(\varepsilon_r - \sin^2\theta)^{1/2}]} . \tag{3.32}$$

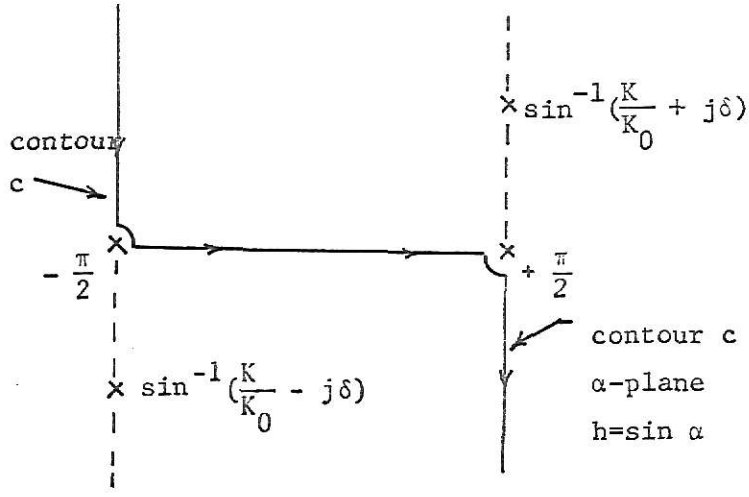

Figure 3.13 *Transformation* h = sin α showing new contour.

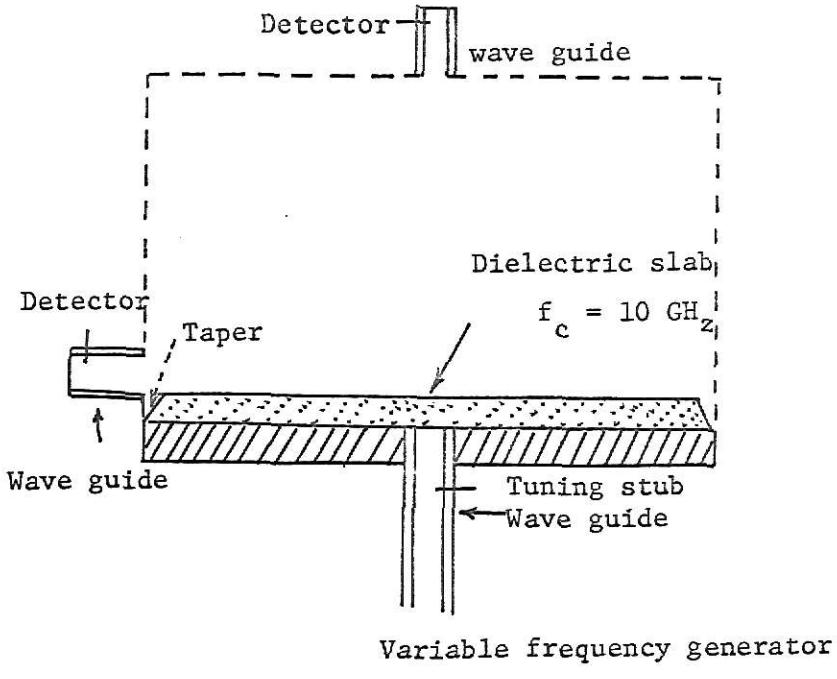

Fig. 3.14 Apparatus for measuring broadside and end-fire radiation

$T(\theta)$ is dependent on θ and changes the radiation pattern of the aperture for all angles to some extent. However, the most significant changes occur at angles near $\theta = \frac{\pi}{2}$, and at the frequencies in the vicinity of cutoff for a TE_n surface wave on a dielectric slab covering a ground plane.

The distortion of the radiation pattern has the physical appearance of a surface wave. The radiation energy is near the dielectric interface; however, it is quite different in several respects. First, the radiation which is discussed here belongs to the continuous spectrum of the aperture radiation field. Its amplitude decays inversely with respect to the distance from the aperture, rather than being independent of distance. Furthermore, the endfire radiation does not exhibit a cutoff characteristic but has a symmetrical amplitude variation about the frequencies given by equation (3.32).

The surface wave modes excited by the aperture are associated with the discrete spectrum of the radiation field, and are derived mathematically from the residues of the inversion integral with respect to its poles. These poles correspond to solutions of the equation

$$\cos \beta t + \frac{\alpha_0}{\beta} \sin \beta t = 0 \qquad (3.33)$$

where $\alpha_0 = (h_0^2 - K_0^2)^{1/2}$, h_0 being the surface wave propagation constant.

Experimental work on this problem has been done by using an apparatus as illustrated in Figure 3.14, which consists of a network feeding an open X-band (WR-90) waveguide flanged to a ground plane. In order to simulate the two dimensional situation, parallel conducting planes in the H-plane

are used. No additional field components are induced, and the fields are independent of the position in the E-plane.

The ground plane and aperture are covered by a uniform slab of stycast material with dielectric constant of 6.0 and thickness such that the $(TE)_1$ mode cutoff frequency was 10.0 GHz. The experimental results shown in Figure 3.15 demonstrate the resonant end-fire radiation phenomenon. The peak of end-fire signal at 10 GHz is the same as that obtained in the theoretical curve. The first principal effect of the sheath on the pattern of a matched element is to introduce a broadening of the radiation pattern and a resulting component of radiation in the endfire direction at frequencies near the cutoff frequency of a surface wave on the dielectric slab. However, it is important to distinguish this phenomenon, which is regarded as a distortion of the far-zone radiation pattern, from what is commonly referred as a surface wave, which is a separate mode of propagation belonging to the discrete spectrum of the radiation field.

3.4 Integral Equation Method. This method expands the field into appropriate normal modes in the various regions and then matches boundary conditions across the interfaces. The structure of the infinite array of rectangular wave guides discussed in this method is similar to that of Figure 3.1. In this method, the array structure is also chosen as a two dimensional array fed by parallel plate waveguides and the structure is also considered infinite in both the x and y directions. The differences between Figure 3.2 and Figure 3.16 are the following. Figure 3.2 has a symmetric iris in the aperture and the width of the slot is chosen very small. Figure 3.16 does not have an iris in the aperture and the width

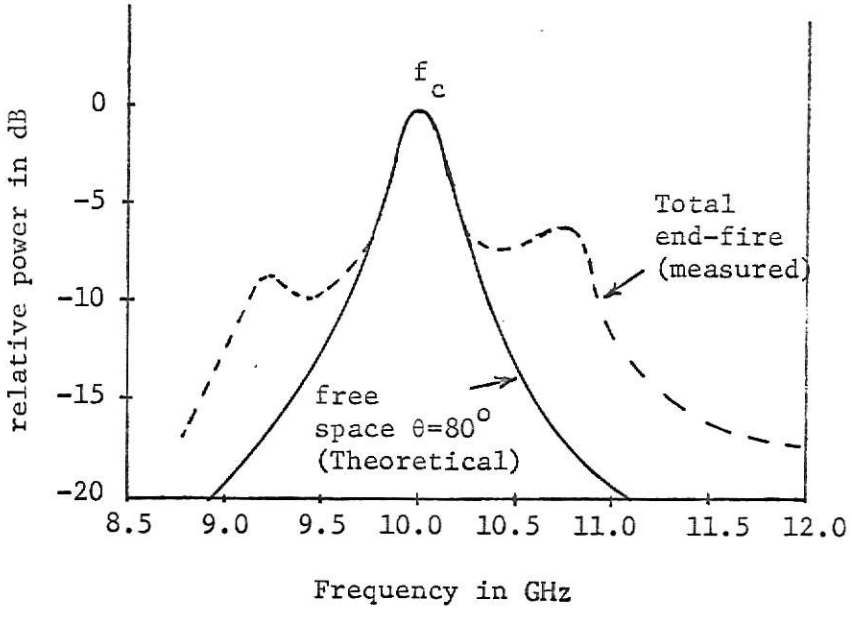

Fig. 3.15. Observed end-fire radiation under-matched conditions

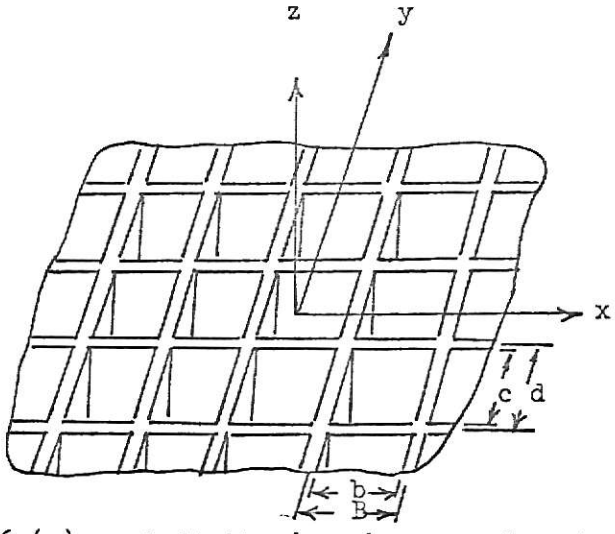

Figure 3.16 (a) an infinite phased array of rectangular wave guide

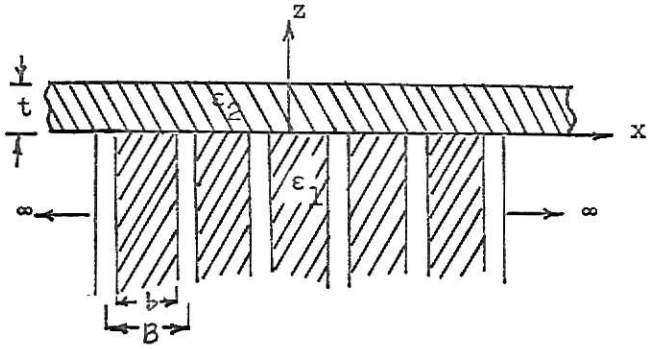

Figure 3.16 (b) a parallel plate phased array covered by a dielectric sheath

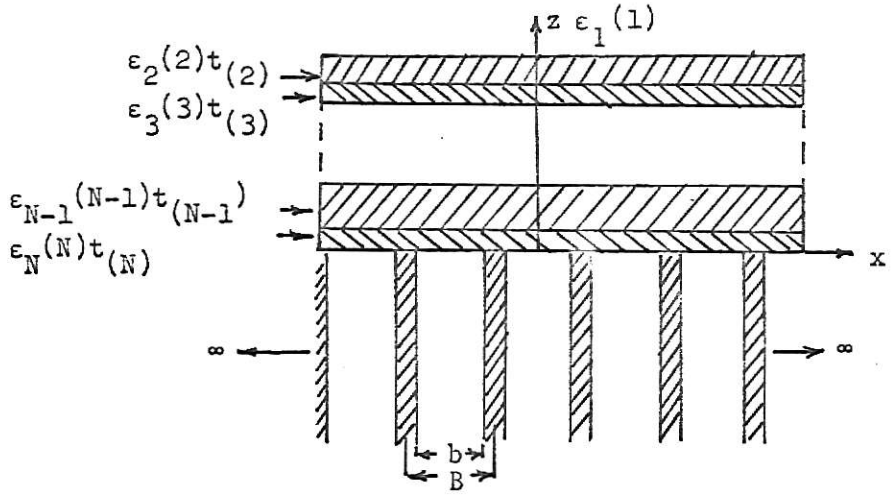

Figure 3.17 Radiation of an array through N dielectric sheath

of the slot is as wide as the parallel plate waveguide. Also, the medium in the parallel plate waveguide of Figure 3.2 is filled with air, while the medium of the parallel plate waveguide of Figure 3.16 is filled with a dielectric material. In order to consider an infinite array of parallel plates covered with a single dielectric slab and scanned in the H-plane as shown in Figure (3.16b), it is convenient to divide the space into three regions, the region inside the waveguides, the region inside the dielectric slab, and the region in free space. However, regarding the geometry of the problem, it suffices to separate the space into two regions, inside and outside the waveguide.

The orthonormal functions and the modal impedances in the feed waveguide are given by

$$\phi_n(x) = \sqrt{\frac{2}{b}} \cos\left(\frac{n\pi}{b} x\right) , \quad \text{if } n = \text{odd} \quad |x| \leq \frac{b}{2}$$

$$\phi_n(x) = \sqrt{\frac{2}{b}} \sin\left(\frac{n\pi}{b} x\right) , \quad \text{if } n = \text{even} \quad |x| \leq \frac{b}{2}$$

$$\phi_n(x) = 0 \qquad \text{for } \frac{b}{2} \leq |x| \leq \frac{B}{2}$$

and

$$Z_n = \omega\mu/\alpha_n$$

where

$$\alpha_n = \sqrt{K^2\epsilon_1 - \left(\frac{n\pi}{2}\right)^2} , \quad n = 0, 1, 2, 3 \ldots$$

$$K = \omega\sqrt{\mu_0\epsilon_0}$$

and α_n is the z-directed propagation constant for a waveguide filled with a dielectric of dielectric constant ϵ_1. By using the Floquet theorem

(Collin, 1960), it can be shown that the dielectric slab region and the free space region have identical modal functions when the tangential fields are continuous at all points across the dielectric-free space interface. The normalized modal functions can take the form:

$$\psi_m(x) = \sqrt{\frac{1}{B}} \exp\{j((2m\Pi/b) + T_x)x\} \qquad m = 0, \pm 1, \ldots$$

where T_x is the phase shift per unit length. The modal impedances for the dielectric and free space regions are different. They are given respectively by

$$Z_m^D = \omega\mu/\beta_m,$$

$$\beta_m = \sqrt{K^2\varepsilon_2 - \left(\frac{2m\Pi}{B} + T_x\right)^2} \qquad \text{for } 0 \leq z \leq t$$

and

$$Z_m^0 = \omega\mu/\gamma_m,$$

$$\gamma_m = \sqrt{K^2 - \left(\frac{2m\Pi}{B} + T_x\right)^2} \qquad \text{for } z > t$$

When the waveguide is excited in the fundamental mode with unit amplitude, the fields in various regions are expanded into the normal modes and can be written as

$$H_x(x,z) = (e^{j\alpha_1 z} + R\, e^{-j\alpha_1 z})\, \phi_1(x) + \sum_{n=2}^{\infty} I_n \phi_n(x)\, e^{-j\alpha_n z}, \quad z \leq 0$$

$$H_x(x,z) = \sum_{m=-\infty}^{\infty} (I_m^+ e^{j\beta_m z} + I_m^- e^{-j\beta_m z})\, \psi_m(x), \quad 0 \leq z \leq t$$

$$H_x(x,z) = \sum_{m=-\infty}^{\infty} I_m'\, \psi_m(x)\, e^{j\gamma_m (z-t)}, \quad z \geq t$$

and

$$E_y(x,z) = -Z_1(e^{j\alpha_1 z} - R\, e^{-j\alpha_1 z})\, \phi_1(x) + \sum_{n=2}^{\infty} Z_n I_n \phi_n(x)\, e^{-j\alpha_n z}, \quad z \leq 0$$

(3.35)

$$E_y(x,z) = -\sum_{m=-\infty}^{\infty} Z_m^D (I_m^+ e^{j\beta_m z} - I_m^- e^{-j\beta_m z})\, \psi_m(x), \quad 0 \leq z \leq t$$

$$E_y(x,z) = -\sum_{m=-\infty}^{\infty} Z_m^0 I_m' \psi_m(x)\, e^{j\gamma_m (z-t)}, \quad z \geq t$$

where R = reflection coefficient.

Z_m^D = the modal impedance in dielectric

Z_m^0 = the modal impedance in free space

The I's are the unknown modal coefficients. Waves of all modes travelling in both the positive and negative z directions are included in the fields for $0 \leq z \leq t$, because this region is situated between two interfaces. Similarly, the fields for $z \leq 0$ contain components travelling in the negative z-direction due to scattering at the array aperture.

By applying the boundary conditions at z = 0, the following equations can be found

$$H_x(x) = H_x(x,0) = (1+R)\phi_1(x) + \sum_{n=2}^{\infty} I_n \phi_n(x)$$

$$= \sum_{m=-\infty}^{\infty} (I_m^+ + I_m^-) \psi_m(x) \tag{3.36}$$

$$E_y(x) = E_y(x,0) = -Z_1(1-R) \phi_1(x) + \sum_{n=2}^{\infty} Z_n I_n \phi_n(x)$$

$$= - \sum_{m=-\infty}^{\infty} Z_m^D (I_m^+ - I_m^-) \psi_m(x)$$

Because of the orthonormality among the modal functions, one obtains

$$(1+R) = \int_{-b/2}^{b/2} \phi_1(x) H_x(x) dx,$$

$$I_n = \int_{-b/2}^{b/2} \phi_n(x) H_x(x) dx, \qquad n \geq 2 \tag{3.37}$$

$$I_m^+ + I_m^- = \int_{-b/2}^{b/2} \psi_m(x) H_x(x) dx$$

Similarly, from the boundary condition at the interface, z = t,

$$H_x(x,t) = \sum_{m=-\infty}^{\infty} (I_m^+ e^{j\beta_m t} + I_m^- e^{-j\beta_m t}) \psi_m(x)$$

$$= \sum_{m=-\infty}^{\infty} I_m' \psi_m(x) \tag{3.38a}$$

$$E_y(x,t) = \sum_{m=-\infty}^{\infty} Z_m^D (I_m^+ e^{j\beta_m t} - I_m^- e^{-j\beta_m t}) \psi_m(x)$$

$$= - \sum_{m=-\infty}^{\infty} Z_m^0 I_m' \psi_m(x) \tag{3.38b}$$

By observing the right and the left side of equations (3.38a) and (3.38b) which are expanded with respect to the same set of modal functions, one may write

$$I_m^+ e^{j\beta_m t} + I_m^- e^{-j\beta_m t} = I_m' \tag{3.39a}$$

$$Z_m^D (I_m^+ e^{j\beta_m t} - I_m^- e^{-j\beta_m t}) = Z_m^0 I_m' \tag{3.39b}$$

Equations (3.39a) and (3.39b) show that the air-dielectric interface at z = t is a simple one in that the m-th order mode in the dielectric region couples only into the same order mode in the free space region. This implies that the fields at the air-dielectric interface are completely determined when the fields at the array aperture are obtained. Hence, it is necessary to solve only for the aperture field. From equations (3.35), (3.36), (3.39a) and (3.39b) one obtains an integral equation having only the aperture magnetic field as the unknown function. Thus

$$2Z_1 \phi_1(x) = \int_{-b/2}^{b/2} \left\{ \sum_{n=1}^{\infty} Z_n \phi_n(x)\phi_n(x') + \sum_{m=-\infty}^{\infty} Z_m' \psi_m(x)\psi_m(x') \right\} H_x(x')\, dx' \tag{3.40}$$

where

$$Z_m' = Z_m^D \frac{Z_m^0 - jZ_m^D \tan \beta_m t}{Z_m^D - jZ_m^0 \tan \beta_m t} \tag{3.41}$$

It is clear from equation (3.41) that the equivalent impedance Z_m' for the m^{th} order modes is the familiar input impedance of a transmission

line which has a characteristic impedance Z_m^D, propagation constant β_m and length t, and is terminated in a load impedance Z_m^0.

If one wishes to study the property of an array covered by a stratified medium as shown in Figure 3.17, equation (3.40) is still a valid integral equation. In this case, Z_n are the waveguide mode impedances, and Z_m' are the modal impedances which are seen at the array aperture of the N layer stratified dielectric medium.

According to the Floquet theorem, the exterior modal functions for the quasi-E plane scan are the same as those for H-plane scan, but the wave modes supported by the waveguide are different. The orthonomal modal functions for this scan are

$$\omega_n(y) = -\sqrt{\frac{\varepsilon_n}{c}} \cos\left(\frac{n\pi}{c} y\right), \quad n = \text{even}, \quad \text{for } y \leq \frac{c}{2}$$

$$\omega_n(y) = -\sqrt{\frac{\varepsilon_n}{c}} \sin\left(\frac{n\pi}{c} y\right), \quad n = \text{odd}, \quad \text{for } y \leq \frac{c}{2}$$

$$\omega_n(y) = 0 \qquad \text{for } \frac{c}{2} \leq y \leq \frac{d}{2}$$

where

c = internal waveguide width

d = element spacing

A sinusoidal variation of sin [(π/d)x] which applies to all tangential field components, is omitted for brevity.

The integral equation, with the aperture electric field as the unknown, can be given by

$$2Y_0\omega_0(y) = \int_{-c/2}^{c/2} \left\{ \sum_{n=0}^{\infty} Y_n \omega_n(y) \omega_n(y') + \sum_{m=-\infty}^{\infty} Y_m' \psi_m(y) \psi(y') \right\} E_y(y') \, dy' \tag{3.42}$$

where

$$Y_n = \left(K^2\varepsilon_1 - \left(\frac{n\Pi}{c}\right)^2\right)^{\frac{1}{2}}/\omega\mu$$

The Y_n are the interior modal admittances and the Y'_m are the exterior modal admittances with the presence of the dielectric slab.

The method used in solving the integral equations is as follows: The first step is to expand the unknown function as a linear combination of N linearly independent functions. The second step is to substitute the representation into the original integral equation which leads to an approximate equation. The third step is to set the difference between the left and the right side of approximation equations to be orthogonal to the set of functions individually. Then, the fourth step is to obtain a set of N equations in N unknowns. The fifth step is to assume the higher mode coefficients to be zero. The magnetic field is thus assumed to be

$$H_x(x) \simeq \sum_{m=-M}^{M} I'_m \psi_m(x), \qquad I_m = 0 \text{ for } |m| > M \tag{3.43}$$

Substituting (3.43) into (3.40) leads to

$$2Z_1\phi_1(x) - \sum_{m=-M}^{M}\left\{\sum_{n=1}^{\infty} Z_n C_{nm} \phi_n(x) + Z'_m \psi_m(x)\right\} I'_m \simeq 0 \tag{3.44}$$

where

$$C_{nm} = \int_{-b/2}^{b/2} \phi_n(x)\, \psi_m(x)\, dx$$

Because equation (3.44) is orthogonal to the set of functions $\psi_\ell(x)$, $\ell = 0, \pm 1, \ldots \pm M$, it can be shown that

$$\sum_{m=-M}^{M} \left\{ \sum_{n=1}^{\infty} Z_n C_{nm} C_{n\ell} + Z'_m C_{m\ell} \right\} I'_m = 2Z_1 C_{1\ell} \quad \ell = 0, \pm 1, \ldots \pm M. \qquad (3.45)$$

where

$$C_{n\ell} = \int_{-b/2}^{b/2} \phi_n(x)\, \psi_\ell(x)\, dx \ .$$

The reflection coefficient R is then obtained from equations (3.43) and (3.37).

$$(1+R) = I_1 \simeq \sum_{-M}^{M} C_{1m}\, I'_m \ . \qquad (3.46)$$

Figures 3.18 and 3.19 show the reflection coefficients as a function of scan angles for an infinite array of rectangular waveguides which are covered with a single dielectric layer and scaned in the H-plane. The results are obtained for the following parameter values; $b/\lambda = B/\lambda = 0.5714$, $\varepsilon_r = 3.0625$ with different dielectric slab thicknesses t. From those curves one can find that

(i) when the thickness of dielectric slab is very small, no resonant peak occurs.

(ii) When the thickness is increased beyond a critical value, usually in the vicinity of $3\lambda_{\varepsilon_r}/16$ a resonant peak starts to appear at a scan angle close to the value $2\pi(1-b/\lambda)$, and the peak is preceded by a dip.

(iii) Increasing the slab thickness causes the peak to move toward the broadside direction and the peak becomes sharper.

(iv) A further increase in the slab thickness makes more than one peak appear.

For the E plane scan, Figures 3.20 and 3.21 show the amplitude of the reflection coefficient as a function of scan angle with parameter

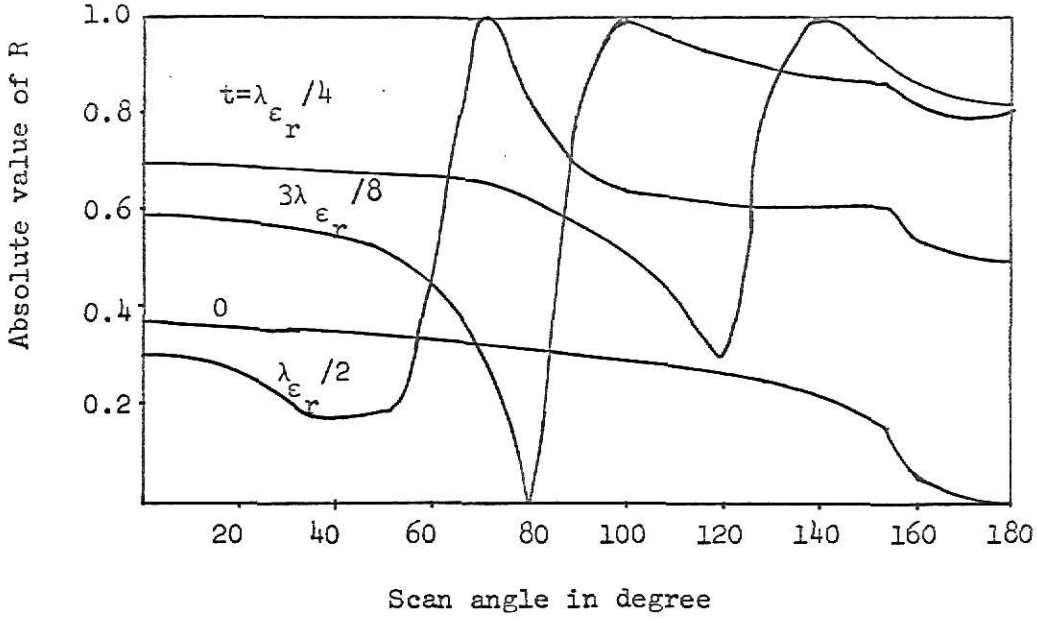

Figure 3.18. Reflection coefficient R vs scan angle TxB for H-plane scan with $B/\lambda = b/\lambda = 0.5714$, and $\varepsilon_r = 3.0625$

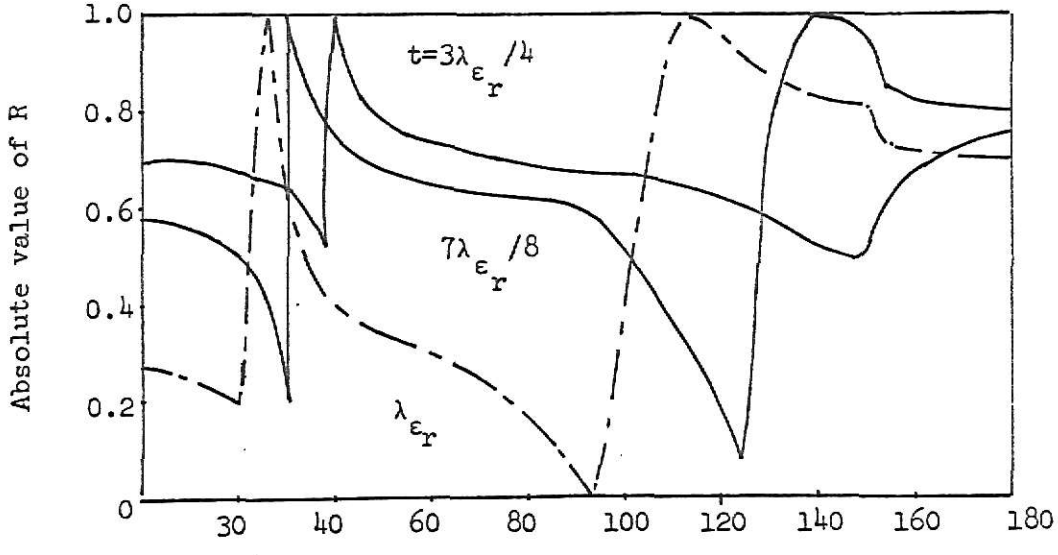

Figure 3.19 Reflection coefficient R vs scan angle TxB for H-plane scan with $B/\lambda = b/\lambda = 0.5714$ and $\varepsilon_r = 3.0625$

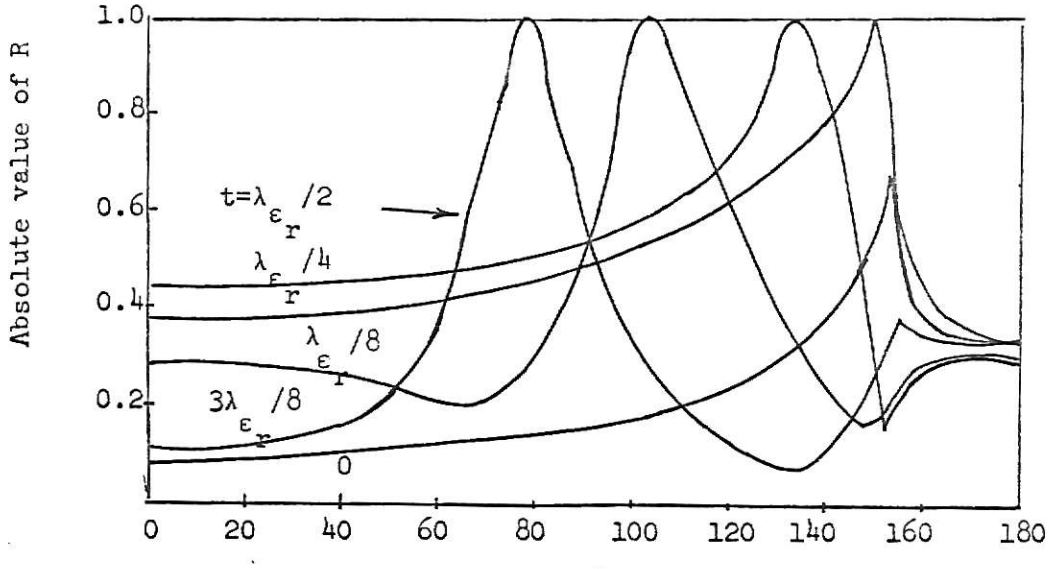

Figure 3.20. Reflection coefficient R vs scan angle Tyd for E-plane scan with $d/\lambda = 0.5714$, $c/d = 0.85$ and $\varepsilon_r = 3.0625$.

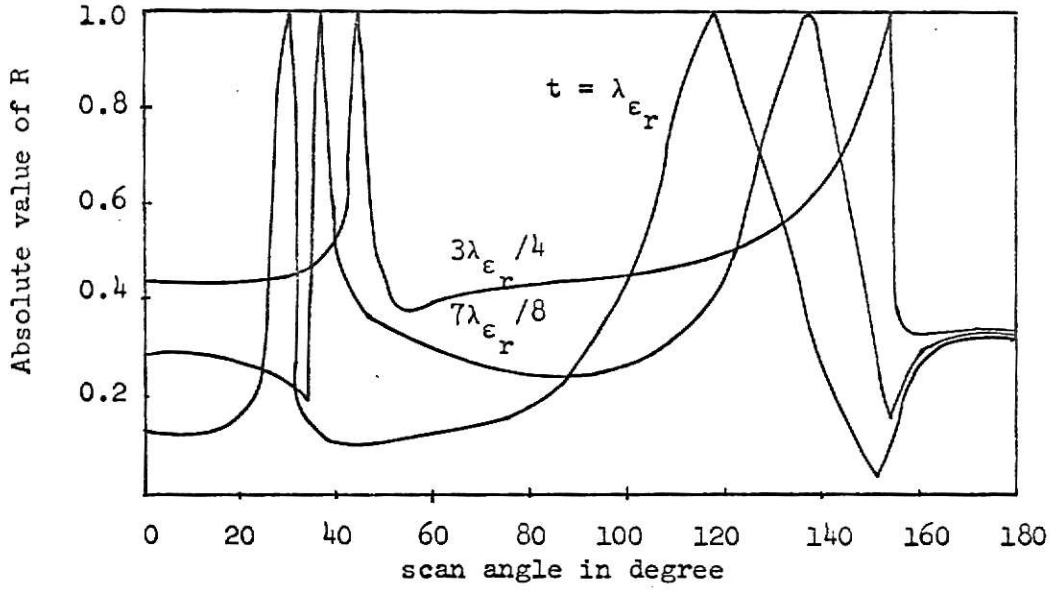

Figure 3.21. Reflection coefficient R vs scan angle for E-plane scan with $d/\lambda = 0.5714$, $c/d = 0.85$ and $\varepsilon_r = 3.0625$

values $d/\lambda = 0.5714$, $\frac{c}{d} = 0.85$ and $\varepsilon_r = 3.0625$. Also, thick waveguide walls are used in order that the waveguides may support only the dominant TEM mode.

From the above analysis, one may find that for the E plane scan, in the absence of a dielectric material, the reflection coefficient is flat over a range of scan angles except in the vicinity of the grating lobe formation angle ($T_y t = 154^o$). At this angle a sharp peak appears. This peak position is not changed as long as the dielectric slab is relatively thin. But as the thickness is increased beyond a critical value of about $\lambda_{\varepsilon_r}/4$, the peak starts to shift toward the broadside direction. A further thickening of the dielectric slab will lead to multiple nulls. This phenomenon is caused by surface-wave-like space harmonics propagating over the corrugated surface.

CHAPTER IV

EXCITATION AND APPLICATION OF SURFACE WAVES

4.1 Typical Surface Waves. For the time being, the surface waves of greatest interest have the following three distinctive forms, namely (i) the inhomogeneous plane wave supported by a flat surface, known as the Zenneck wave; (ii) the inhomogeneous radial cylindrical wave also supported by a flat surface and sometimes described as the radial form of the Zenneck wave; and (iii) the axial cylindical wave (supported by a cylindrical surface) associated with a surface of circular profile in the transverse plane and referred to as the Sommerfeld-Goubau wave. These forms of surface waves are shown in Figure 4.22. All of those field components can be derived from the Maxwell's equations.

First, it is assumed that the surface as shown in Fig 4.22(a) lies in the x-y plane at y = 0 and that the media on each side of the interface are homogeneous. To describe the wave one requires that there exists the three field components E_x, E_y and H_z, both above and below the surface. Naxwell's equations can then be reduced to

$$\frac{\partial E_y}{\partial x} - \frac{\partial E_x}{\partial y} = -j\omega\mu H_z \tag{4.1}$$

$$\frac{\partial E_y}{\partial x} = -\left(\frac{1}{\sigma+j\omega\varepsilon}\right)\frac{\partial^2 H_z}{\partial x^2} \tag{4.2}$$

$$\frac{\partial E_x}{\partial y} = \left(\frac{1}{\sigma+j\omega\varepsilon}\right)\frac{\partial^2 H_z}{\partial y^2} \tag{4.3}$$

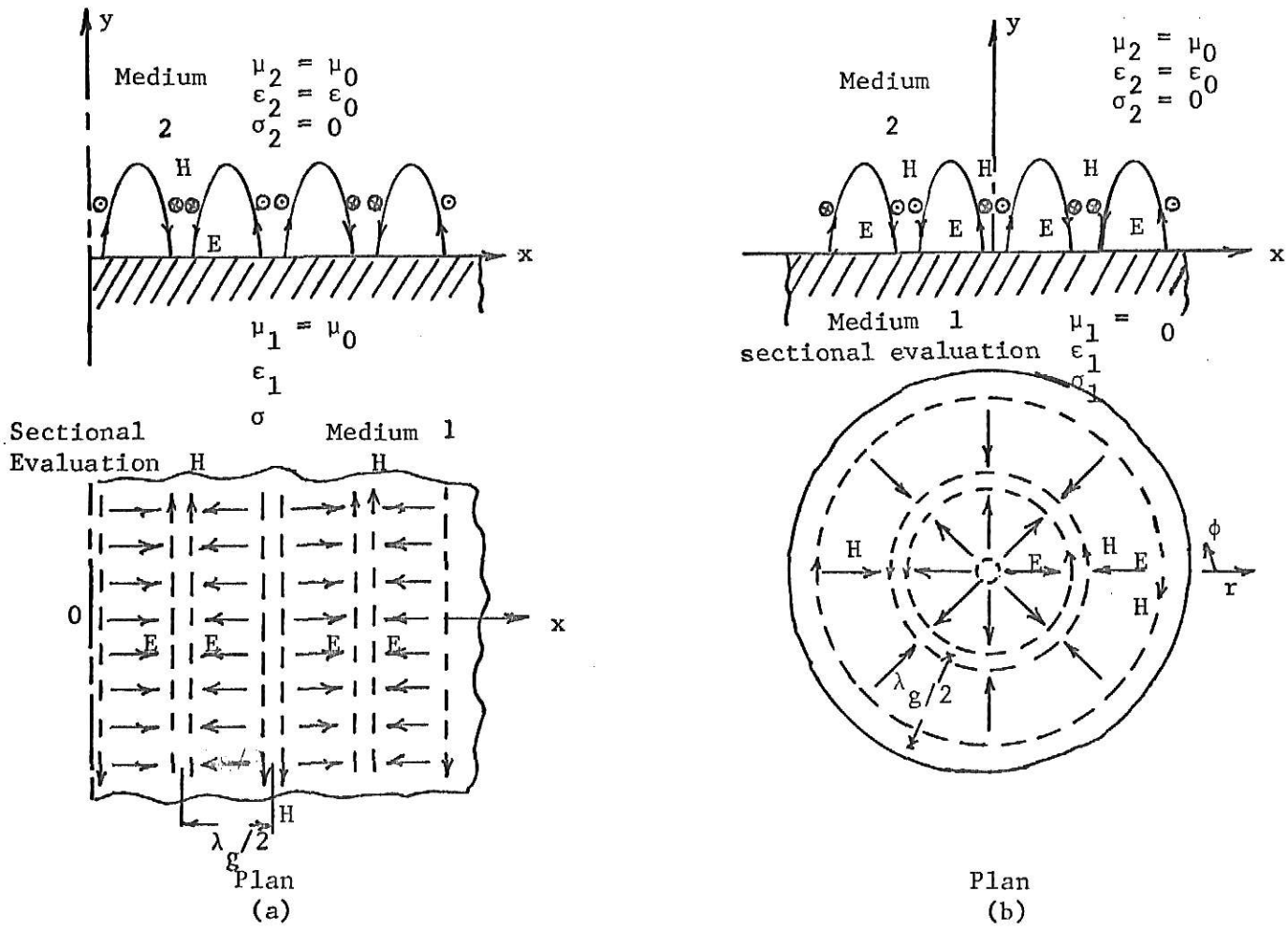

Figure 4.22. Typical Surface Wave

(a) plane wave (b) radial cylindrical surface wave

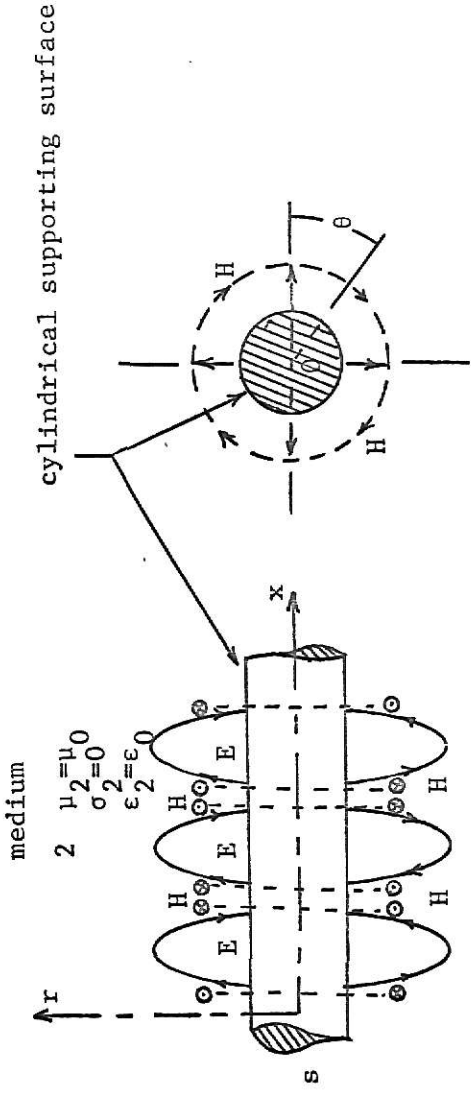

Figure 4.22 (c) Axial cylindrical surface wave

Combining equations (4.1), (4.2) and (4.3), the Zenneck wave equation can be obtained as

$$\frac{\partial^2 H_z}{\partial x^2} + \frac{\partial^2 H_z}{\partial y^2} = - K^2 H_z \tag{4.4}$$

where

$$K^2 = -j\omega\mu(\sigma+j\omega\varepsilon)$$

Secondly, in order to find the corresponding field components E_r, E_y and H_ϕ of the radial cylindrical surface wave as shown in Figure 4.22(b) one can reduce Maxwell's equations in cylindrical coordinates to

$$\frac{\partial E_r}{\partial y} - \frac{\partial E_y}{\partial r} = -j\omega\mu H_\phi \tag{4.5}$$

$$- \frac{\partial H_\phi}{\partial y} = (\sigma+j\omega\varepsilon)E_r$$

$$\frac{1}{r} H_\phi + \frac{\partial H_\phi}{\partial r} = (\sigma+j\omega\varepsilon)E_y \tag{4.7}$$

Combining the equations (4.5), (4.6), and (4.7), the radial cylindrical surface wave equation is obtained

$$- \frac{\partial^2 H_\phi}{\partial y^2} - \frac{\partial^2 H_\phi}{\partial r^2} + \frac{1}{r^2} H_\phi - \frac{1}{r} \frac{\partial H_\phi}{\partial r} = K^2 H_\phi \ . \tag{4.8}$$

where

$$K^2 = -j\omega\mu(\sigma+j\omega\varepsilon)$$

Thirdly, the axial cylindrical wave is shown in Figure 4.22(c) and it has the field components H_θ, E_r, and E_x which can be obtained from the Maxwell's equations

$$\frac{\partial E_r}{\partial x} - \frac{\partial E_x}{\partial r} = -j\omega\mu H_\theta \tag{4.9}$$

$$-\frac{\partial H_\theta}{\partial x} = (\sigma+j\omega\varepsilon)\, E_r \tag{4.10}$$

$$\frac{1}{r} H_\theta + \frac{\partial H_\theta}{\partial r} = (\sigma+j\omega\varepsilon)\, E_x \tag{4.11}$$

Combining equations (4.9), (4.10) and (4.11), one can obtain the axial cylindrical surface wave equation.

$$-\frac{\partial^2 H_\theta}{\partial x^2} - \frac{\partial^2 H_\theta}{\partial r^2} + \frac{1}{r^2} H_\theta - \frac{1}{r}\frac{\partial H_\theta}{\partial r} = K^2 H_\theta \tag{4.12}$$

where

$$K^2 = -j\omega\mu(\sigma+j\omega\varepsilon)$$

The solutions of equations (4.4) and (4.8) can be found by seeking for an exponential decay of field above and below the surface. Equation (4.12) can be solved by using the standard form of Bessel's equation. The details of solutions of these three fundamental forms of surface waves have been studied by Barlow and Brown (1962). The axial cylindrical surface wave is regarded as perhaps the most important form of surface wave from the point of view of application.

4.2 Excitation and Application of Surface Waves. In recent years, because there still exists various problems of launching surface waves in

transmission systems, surface waves have not been widely used. The problem of launching has been considered in various aspects. Theoretically an infinite aperture is required to launch a pure surface wave, but in practical cases a good approximation to this requirement is obtained by means of a horn-type radiator spreading out a TEM wave source. This technique can be applied as shown in Figure 4.23, not only to the plane and radial form of Zenneck wave, but also to the axial cylindrical wave. The efficiency of launching an axial cylindrical wave is relatively high because the field distribution of the TEM wave from the coaxial line source, being inversely proportional to the radius, forms a better match to the corresponding surface wave Hankel function distribution. There are also other kinds of launchers, such as dipoles and slots. The two types of launchers can be mounted at appropriate heights above the guide surface. In suitable circumstances, the launching efficiency can be as high as 80 percent (see Figure 4.24). The axial cylindrical wave as a high-frequency link between two points has many applications. The single-wire transmission line can be suspended by nylon cords, so as to keep the wire away from obstacles disturbing the free passage of the wave. It is generally convenient to coat the wire with a layer of dielectric in order to confine most of energy of the field within a reasonable distance outside the wire. An installation of this kind has been set up over the McDonald Pass in Montana, U.S.A. as a television link. The line is 14 miles long and operated in the frequency range of 150 to 250 MHz with an attenuation averaging 10dB per mile.

Surface waves on single-wire transmission lines are not subject to a frequency cut-off and theoretically they can be used in any part of the

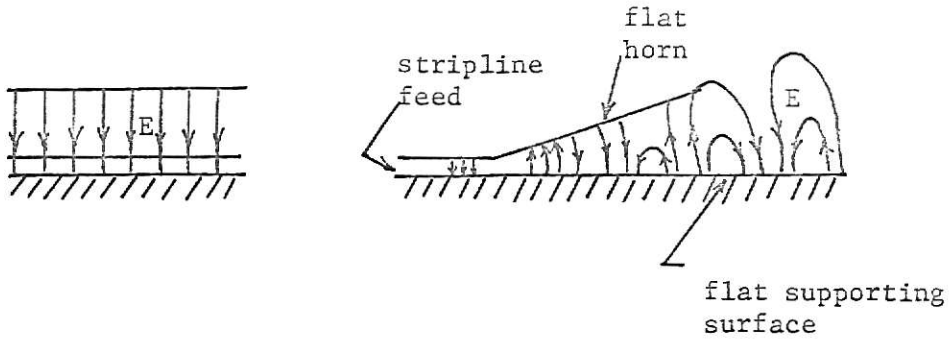

(a) Plane Wave

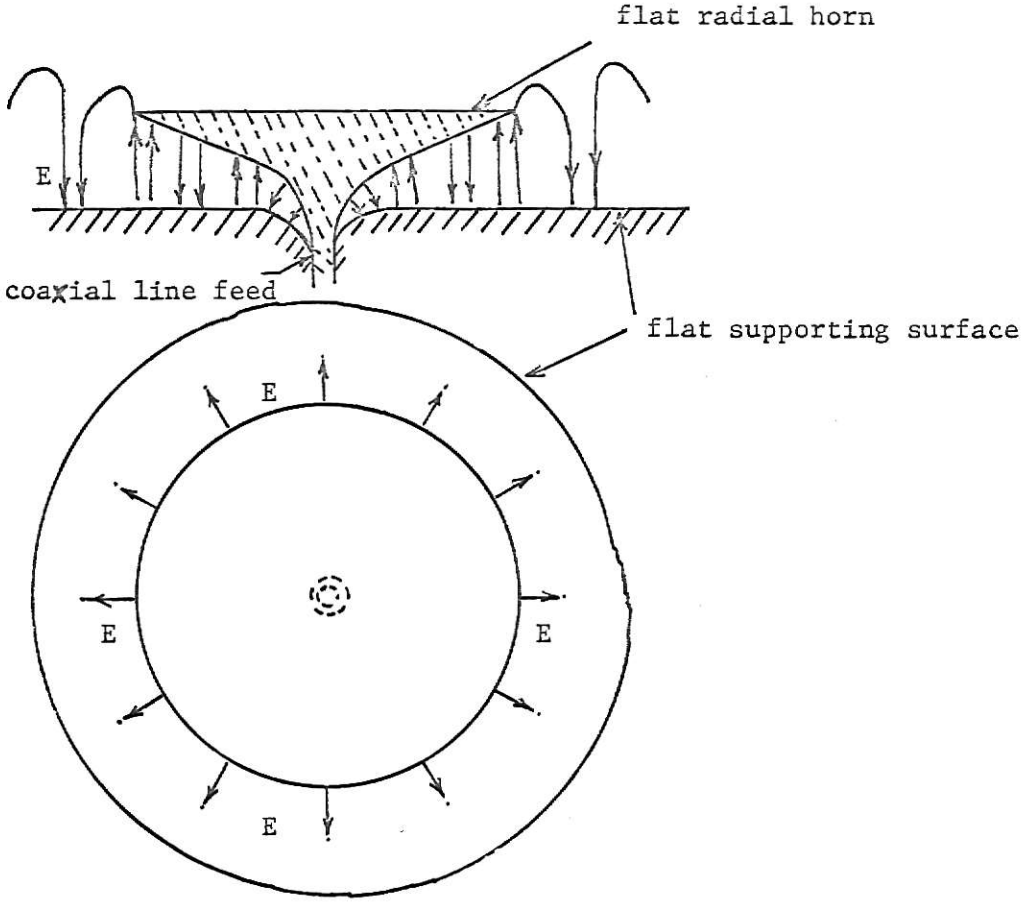

(b) Radial wave over flat surface

Figure 4.23 Horn-Type radiators for launching surface wave

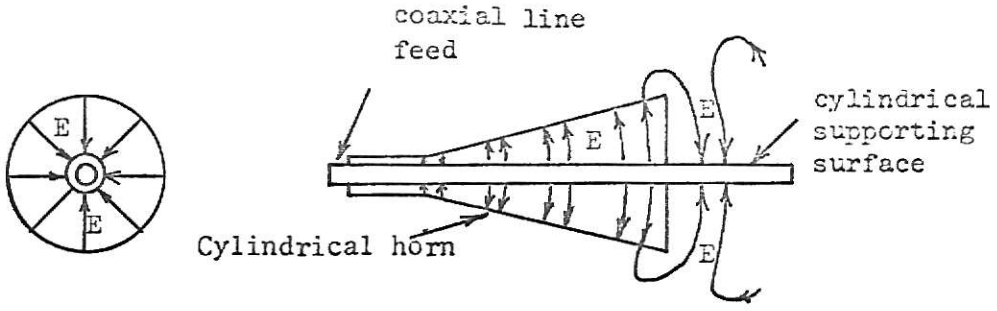

Fegure 4.23 (c) coaxial cylindrical wave

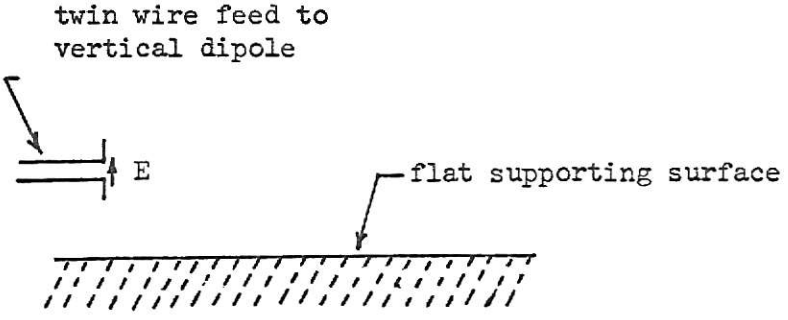

(a) vertical dipole launcher over flat surface

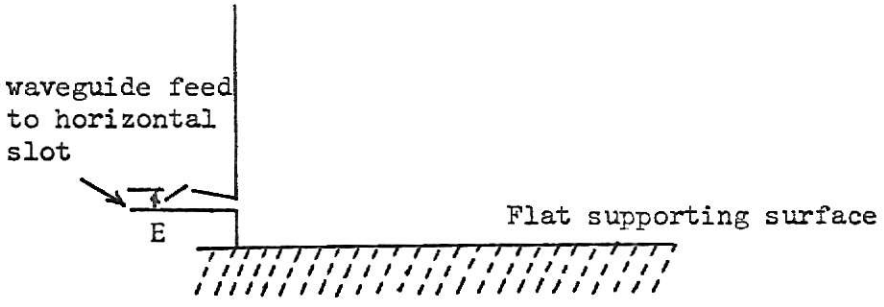

(b) Horizontal launcher over flat surface

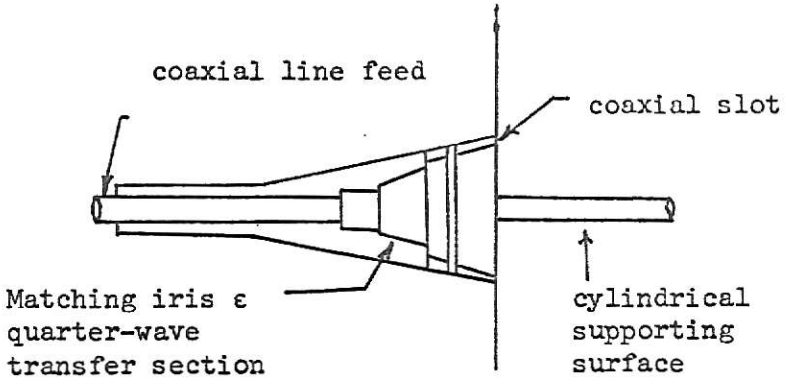

(c) coaxial slot launcher over cylindrical surface

Figure 4.24 Dipole and Slot Launcher

spectrum. In practice, the spread of the field outside the conductor becomes excessive below about 30 MHz, so that a compromise is generally adopted by working in the V.H.F. band. One disadvantage is the fact that the surface wave circuit forms an unscreened channel which can be seriously disturbed by any discontinuity along its length, including sharp bends or water, ice and snow adhering to the surface of the guide.

Under suitable conditions, the Zenneck form of wave can be supported by the sea and might be used for short range communication between ships. Because radiation occurs for surface waves transmitted along guides with suitable discontinuities, such guides can be used as radiators.

There are many antenna structures called surface wave antennas which have been found to support surface waves. Some surface wave antennas can be applied to aircraft, the radiator being mounted nearly flush with the aircraft surface. According to the form of the radiator, those structures are divided into two categories, line radiators and planar radiators. Line radiators consist of dielectric rods, corrugated rods, slotted waveguides, helices, and Yagi-Uda arrays. Planar radiators are dielectric sheet antennas, corrugated surface antennas, ferrite and plasma sheet antennas and slotted surface wave structures. Launching a surface wave over the earth has been done by using a ferrite-loaded horn type of antenna (Barlow, 1967). This type of antenna has been used to launch a 1.5 MHz surface wave over the earth.

CHAPTER V

SUMMARY AND RECOMMENDATION

5.1 Summary. Chapter II starts with the basic concept of electric field components of an incident wave. Instead of introducing the angles of incidence and reflection explicity, the incident wave and transmitted waves in different regions are obtained. By solving the wave equations, the wave impedances at different interfaces are also obtained. Using transmission line theory, the input impedance at the dielectric interface can be represented as an equivalent transmission circuit. By assuming the dielectric is low-loss and the thickness t is very small, one can derive the wave number and propagation factor in terms of the dielectric constant and dielectric thickness t. Thus the characteristics of surface wave propagation along the thin dielectric coated conducting plane are determined.

The thick dielectric coated conducting plane is treated elsewhere by Collin (1960) by means of a complicated mathematical analysis.

Chapter III forms an important part of this report. By using various mathematical methods the effect of surface waves on phased array antenna structures is discussed. The first section discusses the unit cell and equivalent network method. The early history of speculation on the role of surface waves has been summarized by Oliner and Malech (1966). These authors also presented a "ghost mode" hypothesis to explain the cause of the nulls on dielectric-coated slot arrays, and indicated that the surface wave was a mode of a modified short circuit structure. Later, Knittel, Hessel and Oliner (1968) have expanded these early efforts by using the

unit cell and equivalent network method to show the presence of element pattern nulls which occur at certain scan angles on the phased array. The method used to examine the presence of guided waves on phased array surfaces is also mentioned. They have also drawn the conclusion that surface waves can exist on a phased array which is covered by a dielectric slab.

The second section of chapter III uses the Fourier Transform method to investigate the relation between the far-zone radiation pattern and surface waves in an aperture covered by a dielectric sheath. If the distortion of the radiation pattern has the physical appearance of a surface wave, its energy should be near the dielectric interface, but actually it is quite different in several respects. First, the radiation discussed in this section belongs to the continuous, rather than to the discret spectrum of the aperture radiation field. Secondly, its amplitude decays inversely with distance from the aperture. Thirdly, the end-fire radiation does not exhibit a cutoff characteristic but instead has essentially a symmetrical amplitude variation about the frequency given by equation (3.32). The surface wave modes excited by the aperture are associated with the discrete spectrum of radiation field and derive mathematically from the residues of the inversion integral with respect to its poles.

The third section of chapter III uses the integral equation method to analyze the effect of dielectric slabs on the characteristics of phased array antenna structures. According to the theoretical calculations by Wu and Galindo at different wave lengths, the following conclusions are obtained:

(i) When the thickness of dielectric slab is relatively small, no surface wave occurs.

(ii) When the thickness is increased beyond a critical value, usually in the neighborhood of $3\lambda\varepsilon_r/16$ a resonant peak in the reflection of coefficient starts to appear at a scan angle close to the value of $2\pi(1-b/\lambda)$ and the peak is usually preceded by a dip where the surface wave appears.

(iii) When the slab thickness is increased, the peak becomes sharper and moves toward the broadside direction.

(iv) A further increase in slab thickness makes more than one peak appear.

Thus the appearance of a peak in the reflection coefficient is caused by a surface wave at the interface between the dielectric and free space.

Chapter IV contains typical surface wave equations derived from Maxwell's equation and the typical surface wave mode patterns. Also many radiators and launchers for surface waves are mentioned. Among these structures the efficiencies have not been computed by mathematical formula because their geometrics are very complicated. In practice only the Zenneck wave and axial cylindrical wave have a reasonable efficiency using a horn type radiator.

5.2. Recommendations for further study. There still are many difficulties with the excitation of radial cylindrical surface waves on a dielectric-coated conducting plane. The most important problem is the launching efficiency of surface wave power on the conducting plane covered by a layer of dielectric or over a corrugated surface. This problem has been discussed by a number of authors.

ACKNOWLEDGMENTS

The author wishes to express his sincere appreciation to Professor Gary L. Johnson for his constant enthusiasm, kind advice and helpful guidance throughout this work. He also wishes to express his appreciation to Professors Dale E. Kaufman and Leo A. Wirtz for their comments and suggestions to improve this report.

A SELECTED BIBLIOGRAPHY

Attwood, S.S. (1954). "Surface Wave Propagation Over a Coated Plane Conductor." J. Appl. Phys. Vol. 22, pp. 504-509.

Barlow, H.M. (1967). "Launching a Surface Wave Over the Earth." Electronics Letters, Vol. 3 No. 7, p. 304.

Barlow, H.M. and Brown, J., Editor. (1962). "Radio Surface Waves." Oxford: The Clarence Press .

Bobrovnikov, M.S., Goshin, G.G. and Smirnov, V.P. (1965). "Some Problems in Effective Excitation of Radial Cylindrical Surface Waves." Radio Engineering and Electronics Physics. pp. 875-880, vol. 8.

Collin, Robert E. (1960) "Field Theory of Guided Waves." New York: McGraw-Hill, 453-507.

Diamond, B.L. (1967). "Resonance Phenomena in Waveguide Arrays." IEEE G-AP Internat'l Symp. Digest, pp. 110-115.

Deschamp, G.A. (1960) "Determination of Reflection Coefficient and Insertion Loss of a Waveguide Junction." In "Radio Surface Waves", Barlow and Brown Ed. Oxford: The Clarence Press, pp. 114-115.

Farrell, G.F. and Kuhn, D.H. (1966) "Mutual Coupling Effects of Triangular-grid Arrays by Modal Analysis". IEEE. Trans Antennas and Propagation vol 14, pp. 652-654.

Galindo, V. and Wu, C.P. (1968) "Dielectric Loaded and Covered Rectangular Waveguide Phased Arrays". The Bell System Technical Journal, Vol. 47, Jan. 1968, pp. 93-116.

Goubau, G. (1951) "Single Conductor Surface Wave Transmission Lines". Proceedings I.R.E., Vol. 11, June 1951, pp. 619-624.

Harrington, Roger F. (1961). "Time-Harmonic Electromagnetic Fields". New York: McGraw-Hill, pp. 168-169.

Knittel, George H., Hessel, Alexander and Oliner, A.A. (1968). "Element Pattern Nulls in Phased Arrays and Their Relation to Guided Waves". Proceedings of IEEE, Vol. 56, No 11, pp. 1822-1836.

Lechtrick, L.W. (1968). "Effect of Coupling Accumulation in Antenna Arrays" IEEE Trans. Antenna and Propagation, Vol. 16, pp. 31-37.

Nagelberg, Elliott R. (1968). "Radiation Properties of Dielectric Covered Aperture" The Bell System Technical Journal, Vol. 51, May 1968, pp. 2169-2180.

Oliner, A.A. and Malech, R.G. (1966). "Speculations on the Role of Surface Waves". in Microwave Scanning Antennas Vol. 2, R.C. Hensen, Ed. New York: Academic Press, pp. 308-322.

Oliner, A.A. (1963). "Leaky Waves in Electromagnetic Phenomena" Electromagnetic Theory and Antenna, E.C. Jordan, Ed. Vol 2, p. 837.

Silver, S. Editor (1963). "Radio Waves and Circuits" Amsterdam Elsevier, pp. 86-95.

Walter, Carlton H., Editor. (1965). "Traveling Wave Antennas". New York: McGraw-Hill, 324-341.

Wu, C.P. and Galindo, V. (1968) "Surface Wave Effect on Dielectric Sheathed Phased Arrays of Rectangular Waveguides." The Bell System Technical Journal, Vol. 55, Sept. 1968, pp. 117-142.

SOME ASPECTS OF SURFACE WAVES ON ANTENNA STRUCTURES

by

KUEN TIEN HWANG

B.S. Tatung Institute of Technology, Taipei, Taiwan, 1966

AN ABSTRACT OF MASTER'S REPORT

submitted in partial fulfillment of the

requirements for the degree

MASTER OF SCIENCE

Department of Electrical Engineering

KANSAS STATE UNIVERSITY

Manhattan, Kansas

1970

ABSTRACT

The purpose of this report is to review the characteristics of surface waves on thin dielectric coated conducting planes, to study the effect of surface waves on phased arrays, and to review the typical surface waves equations and the typical wave mode patterns.

The results of analysis show that TM surface waves exist over a thin dielectric coated conducting plane with a surface impedance having an inductive term, while TE surface waves exist over a thin dielectric coated conducting plane with a surface impedance having a capacitive term.

The effect of surface waves on phased arrays has been analyzed by various mathematical methods. The results indicate that dielectric covers of various thicknesses over a phased array can change the radiation pattern significantly at different scan angles. This effect is caused by the existence of surface waves on the phased array. Theoretical analysis and experimental measurements have shown good agreement over a given frequency range near the end-fire direction.

The typical surface wave equations have been derived from Maxwell's equations. These equations yield three typical surface waves. The excitation and application of surface waves are discussed. Different excitation techniques are also shown.